Alexander Preiner, BSc.

Characterization of the Joint Network Geometry and its Influence on the Excavation of the Gleinalmtunnel (2nd tube, Styria, Austria)

Master's Thesis

Submitted in fulfilment of the requirements for the degree of

Diplom-Ingenieur

Master's programme Civil Engineering, Geotechnics and Hydraulics

at

Graz University of Technology

Supervisor

O.Univ.-Prof. Dipl.-Ing. Dr.mont. Wulf Schubert

Institute of Rock Mechanics and Tunneling

Graz University of Technology

Andreas Anjan Buyer, M.Sc. B.Sc.

Institute of Rock Mechanics and Tunneling

Graz University of Technology

Graz, September 2018

EIDESSTATTLICHE ERKLÄRUNG
AFFIDAVIT

Ich erkläre an Eides statt, dass ich die vorliegende Arbeit selbstständig verfasst, andere als die angegebenen Quellen/Hilfsmittel nicht benutzt, und die den benutzten Quellen wörtlich und inhaltlich entnommenen Stellen als solche kenntlich gemacht habe. Das in TUGRAZonline hochgeladene Textdokument ist mit der vorliegenden Masterarbeit identisch.

I declare that I have authored this thesis independently, that I have not used other than the declared sources/resources, and that I have explicitly marked all material which has been quoted either literally or by content from the used sources. The text document uploaded to TUGRAZonline is identical to the present master‘s thesis.

Datum / Date	Unterschrift / Signature

Principle of equality

Due to reasons of legibility, this work does not include gender-specific formulations. However, the used male expressions stand for both genders. (Group, 2018)

Acknowledgements

At first, I would like to thank all people, who supported and accompanied me on this journey to the diploma. My biggest thanks go to my family, especially my parents Manuela and Hubert, who I want to thank from the bottom of my heart. Without their essential financial help and mental support, I would have not been able to finish my studies.

Furthermore, I would like to thank my roommates and best friends Julian Wenger and Torsten Aigner, as well as Bernhard Hopf for their constant support and the great times we experienced together.

I would also like to thank my supervisor Andreas Buyer, who constantly supported me in the course of this master thesis with his fundamental geotechnical knowledge and great interest in my work. Finally, I want to thank Wulf Schubert, who actually stirred my interest in rock mechanics and tunnelling during his lectures.

Danksagung

Zunächst möchte ich allen danken, die mich auf Reise des Weges zum Diplom unterstützt und begleitet haben. Mein größter Dank gilt meiner Familie, insbesondere meine Eltern Manuela und Hubert, denen ich von ganzem Herzen danken möchte. Ohne ihre finanzielle Hilfe und mentale Unterstützung wäre ich nicht in der Lage gewesen, mein Studium erfolgreich abzuschließen.

Außerdem bedanke ich mich bei meinen Mitbewohnern und besten Freunden Julian Wenger und Torsten Aigner, sowie bei Bernhard Hopf für deren stetige Unterstützung und die tollen gemeinsamen Erlebnisse.

Ich möchte auch herzlich meinem Betreuer Andreas Buyer danken, der mich im Rahmen dieser Masterarbeit mit seinem fundierten geotechnischen Wissen, sowie seinem großen Interesse an meiner Arbeit, stets unterstützt hat. Abschließend möchte ich Wulf Schubert danken, der mit seinen Vorlesungen mein Interesse für Felsmechanik und Tunnelbau überhaupt erst geweckt hat.

Abstract

A comprehensive determination and characterization of the joint network in a blocky rock mass is key in rock mechanical engineering, as it has a big influence onto the global rock mass strength as well as the ground system behaviours, like possible overbreak with its consequences on safety and expenses.

In order to accomplish a reliable rock mass characterization, an experienced geologist is crucial. However, manual on site discontinuity mapping is time-consuming and subjective. Therefore, remote sensing techniques have been introduced, with the aim of generating objective, reproducible results in a fraction of the time used for manual mapping on site. Measurements can be performed on outcrops as well as on tunnel faces and walls, delivering orientations and spacing of visible discontinuities. In a subsequent step, it is possible, to calculate the theoretical block sizes as well as block shapes, which are formed by the joint network. Moreover, a kinematical analysis of the joint network can be done for the identification of unstable blocks. This thesis presents an approach, beginning with the identification of the discontinuity network (DN) and ending with a correlation matrix, that allows for the interpretation of possible causes for overbreak. Therefore, digital surface models of a selected tunnel section with a length 315 m are analysed, using three different semi-automatic methods. After that, the identified joint sets are compared to the manually mapped structures from the corresponding geological documentation, in order to choose the best matches. Subsequently, a numerical model is generated using the geometrical parameters of the joint sets, to determine the theoretical block size and shape distribution. To account for blocks caving into the tunnel as a cause for overbreak, a kinematic analysis is performed, using an application based on the block theory, in order to identify unstable blocks. In a last step, a correlation matrix is generated, including several different determined rock mass parameters, like the joint network or tunnel face geometry, as well as parameters derived from the provided geological documentation. Aim is to find parameters, which correlate with a documented overbreak in this underground excavation.

Kurzfassung

Eine umfassende Bestimmung und Charakterisierung des Trennflächennetzwerkes in blockigem Gebirge ist von fundamentaler Wichtigkeit in der Felsmechanik, da es einen großen Einfluss auf die globale Gebirgsfestigkeit und das Gebirgs- und Systemverhalten, wie mögliche Überbrüche und deren Auswirkungen auf Sicherheit und Kosten, hat.
Um eine zuverlässige Gebirgscharakterisierung zu erreichen, ist ein erfahrener Geologe von großer Bedeutung. Die manuelle Trennflächenkartierung vor Ort ist jedoch sehr zeitintensiv und subjektiv. Daher wurden Fernerkundungstechniken eingeführt, die das Ziel haben, objektive, reproduzierbare Ergebnisse in einem Bruchteil der Zeit zu erzeugen, die für das manuelle Kartieren vor Ort benötigt wird. Messungen können sowohl an Aufschlüssen als auch an Ortsbrustflächen und Laibungen durchgeführt werden, um Orientierungen und Abstände von sichtbaren Trennflächen zu liefern. In einem nächsten Schritt ist es möglich, die theoretischen Blockgrößen und -formen zu berechnen, die durch das Trennflächennetzwerk gebildet werden. Darüber hinaus, kann eine kinematische Analyse des Trennflächennetzwerkes zur Identifizierung von instabilen Blöcken durchgeführt werden. Diese Arbeit stellt einen Ansatz vor, der mit der Identifizierung des Trennflächennetzwerkes beginnt und mit einer Korrelationsmatrix endet, die die Interpretation möglicher Ursachen für Überbrüche ermöglicht. Dazu werden digitale Oberflächenmodelle eines ausgewählten Tunnelabschnitts mit einer Länge von 315 m erstellt, und anschließend unter Verwendung von drei verschiedenen semi- automatischen Methoden analysiert. Danach werden die identifizierten Trennflächensets mit den manuell kartierten Strukturen der geologischen Dokumentation verglichen, um die am besten übereinstimmenden Trennflächensets zu finden. Des Weiteren wird ein numerisches Modell unter Verwendung der geometrischen Parameter der Trennflächensets erzeugt, um die theoretische Blockgrößen- und Blockformverteilung zu bestimmen. Um kinematisch freie Blöcke die durch die Schwerkraft in den Tunnel fallen als Überbruch zu berücksichtigen, wird eine kinematische Analyse mit einem Programm basierend auf der Block Theorie durchgeführt, die eine Identifizierung instabiler Blöcke ermöglicht. In einem letzten Schritt wird eine Korrelationsmatrix erstellt, die mehrere verschiedene ermittelte Gebirgsparameter, wie das Trennflächennetzwerk oder die Tunnelgeometrie, sowie Parameter, die aus der bereitgestellten geologischen Dokumentation hervorgehen, enthält. Ziel ist es, Parameter zu finden, die mit den dokumentierten Überbrüchen dieses untersuchten Abschnittes korrelieren.

Table of contents

List of figures

List of tables

Abbreviations

D .....dip angle

DD .....dip direction

IBSD…….theoretical in-situ block size distribution

BSD……. block shape distribution

RMR .....rock mass rating

Q.....rock mass quality

DSE .....discontinuity set extractor

SF .....foliation

IBDI.....image based discontinuity identification

JS .....joint set

DN .....discontinuity network

DoF.....degree of fracturing

Symbols

J_v ..... volumetric joint count [1/m^3]

f ..... Joint set frequency [-]

$\bar{s}$ ..... Mean joint set (normal) spacing [m]

$\tilde{s}$ ..... Median joint set (normal) spacing [m]

σ_s ..... Standard deviation of set normal spacing [m]

p ..... persistence of joints [%]

φ ..... friction angle [°]

1 Introduction

1.1 Problem statement

An accurate and detailed rock mass characterisation is key for adequate designs in rock engineering and therefore to a successful project. Right now, a good characterisation is very dependent on the time on site as well as the experience of the mapping geologist. To be less dependent on highly experienced geologists and to derive objective results, remote sensing techniques, along with further data processing and analysis might be a solution. Although a detailed rock mass characterisation is time consuming and costly, the potential of severe consequences for the crew as well as financial issues can be reduced. With the knowledge that each possible event has an acceptable level of risk, mitigation measures have to be considered, to either eliminate the hazard, reduce the probability of its occurrence, or reduce the consequences.

Current rock mass classification systems (e.g. Barton et al., 1974; Bieniawski, 1973; Hoek et al., 2013; Palmström, 1995) use important ground features and parameters to determine the stability of a tunnel excavation and the required support. All classifications systems have the significance of a proper evaluation of the joint network geometry in common. It is well accepted that the intersection of discontinuities in a jointed rock mass creates in-situ blocks of arbitrary three-dimensional geometry, which might be kinematically free and result in slope and tunnel failures or overbreak (Goodman & Shi, 1995). The joint network geometry also controls the size and shape of in-situ rock blocks, which themselves play an important role on the global properties of a rock mass (Gottsbacher, 2017). Furthermore, they limit the possibilities, how the resultant risks can be controlled, for example, the failure geometry of a rock face and the optimum associated support on surface and restraint strategy (Kalenchuk et al., 2006).

Figure 1.1 illustrates the importance of a careful consideration of the block size and orientation in relation to an underground excavation. The picture on the left shows a block, which is instable despite anchoring measures, since they have not been adapted to the given orientation of the discontinuities. Whilst on the right side, an appropriate number, direction and length of the anchors has been chosen, stabilizing the kinematically free block. Besides safety issues and hazards for the crew, overbreak and therefore financial issues are consequences to consider due to insufficient anchoring.

Figure 1.1: Influence of block size and orientation on tunnel stability (Palmström, 2000).

A quotation that illustrates the importance of the consideration of joints:

"Since joints are among the most important causes of excessive overbreak and of trouble with water, they always deserve careful considerations" Karl Terzaghi (1946)

In order to identify joint networks in a reproducible and objective way, several semi-automatic identification methods (e. g. Buyer & Schubert, 2018; Riquelme et al., 2014) have been established in the past decade. These methods use pixel data of high resolution pictures respectively point clouds of the regions of interest, to identify joints. Furthermore, modern software, such as ShapeMetriX^{3D} (3GSM GmbH, 2018) and Sirovision (Datamine & CSIRO, 2018), enable the determination of joint spacing parameters in a subsequent step. Consequently, it is possible to safely and objectively capture geological features, while avoiding a disruption of the construction activities. As these methods provide a large quantity of data, a better statistical evaluation is possible. Due to that, determined joint network parameters (e.g. block volumes, joint spacing) can be compared and checked for correlations with other parameters, like documented overbreak, fault zones and explosive consumption. Hence, a correlation study is performed in this thesis in order to find correlations regarding the overbreak.

Kalenchuk et al. (2006) developed a numerical method to classify both size and shape distributions of any jointed rock mass using the discrete element modelling software 3DEC (Itasca Consulting Group, 2007). Input parameters, to generate the 3-dimensional model representing the rockmass, are joint spacing, orientation and persistence of the joints. As no accurate determination of these parameters can be made, standard deviations of set normal spacings have to be introduced. The evaluation of the joint sets and their corresponding parameters is done, using real data from the Gleinnalmtunnel (2nd tube) including 3D tunnel face models, the geoloical/geotechnical documentation and a list of the

cyclic advance of a approximatelly 300 m long section. For the analyses, the software ShapeMetriX^{3D} (3GSM GmbH, 2018) is used. After that, a stability analysis, using the software VisKBT (Shi, 2017) is performed, and a correlation matrix, using MS Excel, established.

1.2 Research questions

To address the above mentioned issues, a focus on the determination of block sizes, which are represented as the theoretical in-situ block size distribution (IBSD), and the block shapes, represented as the block shape distribution (BSD), is placed. The blocks are checked for their kinematical freedom and the results are compared with documented geological conditions and explosives consumption per round. The thesis is guided by the following questions:

- Are the IBSD and BSD influencing factors regarding the overbreak?
- How do kinematical free blocks inluence overbreak?
- Correlates the documented overbreak with different factors, like the joint net work geometry, or explosives consumption?

2 State of the Art

2.1 Determination of the rock mass geometry

2.1.1 Joint network

A rock mass consists of discontinuities. In general, “discontinuity” is used as a term, denoting any separation of rock blocks and having zero or low tensile strength. History showed that engineering properties of a rock mass are far more often dependent on the occurring joint network than the strength of the rock itself (Palmström, 2002). Therefore, a knowledge of the type and frequency of joints is more important in many cases than the type of rock itself.
A fractured rock mass can be considered to be made of the following three components:

- fracture network
- matrix block
- inflillings along fractures

A single discontinuity or fracture can be described by its orientation (dip & dip direction), strength parameters (tensile/ shear), persistence, aperture etc. A group of discontinuities with similar orientations form a discontinuity set with a certain set spacing. According to Singhal & Gupta (2010) and ISRM (1978), resp. EN ISO 14689-1 (2016), discontinuities can be characterized by the parameters listed in Table 2.1.
Jouanna (1993) suggests that field investigation methods can be divided into two main parts: 2D and 3D. 2D investigations consider observation made at the surface, rock surface or subsurface level and include scanline-, borehole- and different types or areal surveys. 3D investigations are used to gather bulk volumetric properties involving the inner structure of a fractured rock mass. Below, a brief overview of different investigation methods is given:

- 2D methods: Rock surface observations regarding lithology, structure, fractures and their characteristics; made at surface or subsurface level
  - Scanline surveys
  - Areal surveys on outcrops, pits, trenches etc. including terrestrial geophotogrammetry and remote sensing
  - Borehole surveys including drilling, borehole logging, borehole cameras and formation microscanner methods
- 3D methods: Investigations aimed at bulk volumetric properties of rock mass in 3D

- Hydraulic well tests
- Hydrochemical methods
- Geophysical methods including seismic, electrical, gravity, magentic and georadar

Table 2.1: Characteristic parameters of discontinuities (mod. from Singhal & Gupta, 2010).

Parameter	Description
1. Number of sets	Number of sets of discontinuities present in network
2. Orientation	Attitude of discontinuity present in the network
3. Spacing	Perpendicular distance between adjacent discontinuities
4. Persistence	Trace length of the discontinuity seen in exposure
5. Density	
- linear	Number of fractures per unit length
- areal	Cumulative length of fractures per unit area
- volumetric	Cumulative fractured surface area per unit of bulk rock volume
6. Fracture area and shape	Area of fractured surface and its shape
7. Volumetric fracture count	Number of fractures per cubic meter of rock volume
8. Matrix block unit	Block size and shape resulting from fracture network
9. Connectivity or termination code	Intersection and termination characteristics of fractures
10. Aperture	Perpendicular distance between the adjacent rock-walls of a discontinuity (air or water filled)
11. Asperity	Projections of the wall-rock along the discontinuity surface
12. Wall coatings and infillings	Solid materials occurring as wall coatings and filling along the discontinuity surface

Remote sensing in particular, has become a well-established tool for mapping the joint network in rock mechanics (Gaich & Pischinger, 2016). However, since the manual mapping is still time consuming and not always very detailed, the application of semi-automatic identification procedures gains importance in tunnelling projects (Gaich et al., 2017). A recently developed method is the generation of a digital surface models (DSM) of the visible rock mass of the last blasted round by remote sensing, followed by a semi-automatic joint network identification, using appropriate software tools like DSE (Riquelme et al., 2014) or

Sirovision (Datamine & CSIRO, 2018). Accordingly, it provides objective, reproducible data in a fraction of the time compared to manual mapping with a geological compass.

2.1.2 Estimation of block size and shape distribution

As mentioned above, the intersection of joints forms blocks of different volume and shape. These dimensions are governed by the degree of jointing or the density of joints. Determining the IBSD is still difficult, as there is no insight behind the rock face. Depending on the local condition and the availability of measurements, there are different methods of measuring the block size. For instance, in the planning stage, where there are no visible discontinuities, core drillings and borehole logging etc. have to be carried out, to gather information about the joint network. During construction, however, where the tunnel face and sidewalls are exposed, more precise measurements are possible.

As block size is an important parameter for many rock mass classification systems, many publications are dealing with this parameter (e.g. Barton et al., 1974; Bieniawski, 1973; Hoek et al., 2013; Palmström, 1995). Unfortunately, there is still no satisfying method to determine ISBD, as there are always limitations to all of these approaches.

Palmström (2005) discussed various methods with different input parameters to determine the block size. A focus in his investigations was placed on the correlations between block size and rock quality designation (RQD). RQD gives information about the degree of jointing along a defined[1] section of a borehole drilling(Deere & Deere, 1963). Although the RQD is an important component of rock mass classification systems such as RMR and Q, it gives little information about the joint network itself. Therefore, Palmström (2005) tried to find correlations between RQD and the volumetric joint count (J_v) respectively the block volume V_b. As a result, he stated that there is poor correlation between RQD and other types of block size measurements. Thus, he suggests that both, the Q and RMR classification system would be improved, if block size measurements other than the RQD would be applied. Therefore, he introduced the following equation

$$V_b = \frac{S_1 \cdot S_2 \cdot S_3}{\sin(\gamma_1) \cdot \sin(\gamma_2) \cdot \sin(\gamma_3)} \tag{2.1}$$

where S_1, S_2, S_3 denote the average spacing of the three joint sets, and $\gamma_1, \gamma_2, \gamma_3$ the angles between them (see Figure 2.1 respectively).

[1] usually a section of 1 m length

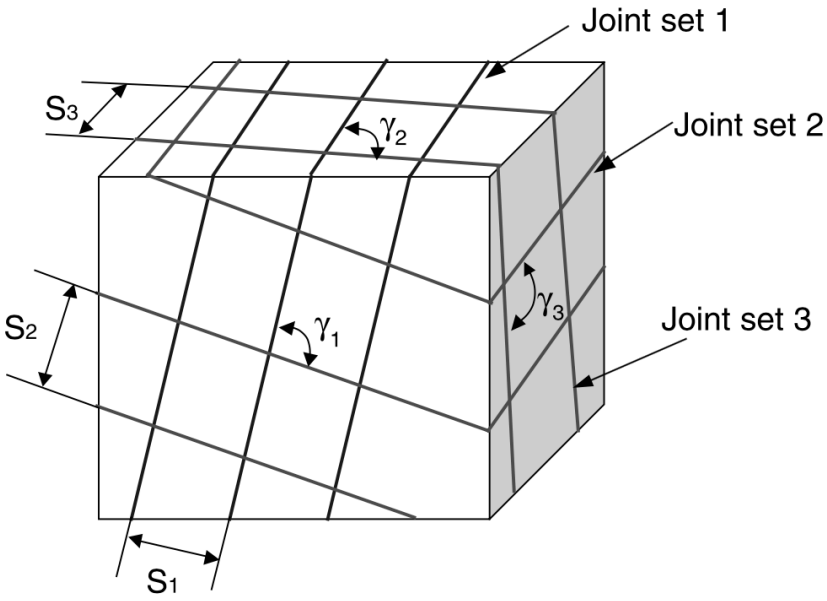

Figure 2.1: Illustration of spacing and angles of the corresponding joint sets (Kim et al., 2007).

A classification of the block volume V_b can be done as follows:

Table 2.2: Classification of the block volume V_b (EN ISO 14689-1, 2016).

Description	Block volume V_b
Very small	10 to 200 cm^3
Small	0.2 to 10 dm^3
Moderate	10 to 200 dm^3
Large	0.2 to 10 m^3
Very Large	> 10 m^3

As shown in equation 2.1, the knowledge of three major joint sets is necessary to apply this formula. In addition, the equation considers joints with a persistence of 100 %. Kim et al. (2007) investigated block size and shape in dependence of the joint persistence and modified the formula for V_b as shown below:

$$V_b = \frac{S_1 \cdot S_2 \cdot S_3}{\sin(\gamma_1) \cdot \sin(\gamma_2) \cdot \sin(\gamma_3) \sqrt[3]{p_1 p_2 p_3}} \tag{2.2}$$

where p_i stands for the persistence of the corresponding joint set. Based on a numerical analysis, where simulated block volumes where compared with the calculated ones, a correlation of ≈ 98 % was achieved, which confirms the validity of the assumption.

If the joint network consists of many random joints, an estimation of the characteristic

dimensions of each block has to be made. In cases of the occurrence of less than three major visible joint sets, a rule of thumb has to be applied by assuming five times the spacing of the visible joint sets. Another method of determining block sizes is the volumetric joint count (Jv). It was first introduced by Palmström in 1972 and is defined as the number of joints intersecting a volume of 1 m^3. It is not limited to a particular number of joint sets

$$J_v = \frac{1}{S_1} + \frac{1}{S_2} + \frac{1}{S_3} + \cdots \frac{1}{S_n}, \tag{2.3}$$

Where S_1, S_2, S_n stand for the average spacing of joint sets. In case of many random joints, Palmström (1982) presented an approximate rule of thumb correction with a spacing of 5 m for each random joint:

$$J_v = \frac{1}{S_1} + \frac{1}{S_2} + \frac{1}{S_3} + \cdots \frac{1}{S_n} + \frac{Nr}{(5\sqrt{A})}, \tag{2.4}$$

where Nr is the number of random joints in a corresponding area A. A classification of the J_v [m^3] displayed is given in the following table:

Table 2.3: Classification of the Jv with regard to the degree of jointing (Palmström, 1982).

	Degree of jointing					
	Very low	Low	Moderate	High	Very high	Crushed
J_v=	<1	1-3	3-10	10-30	30-60	>60

Both, RQD and J_v can only provide average block dimensions and give no accurate block volume or indication of block shape characteristics. Palmström (1995) figured out a correlation between the block size V_b and the volumetric joint count J_v (eq. 2.5).

$$V_b = \beta \cdot J_v^{-3}, ^2 \tag{2.5}$$

where β denotes the block shape factor, which is explained in the following chapter.
Although block shape is not considered in most rock mass characterization methods, it is an influential factor for rock mass behaviour. Gottsbacher (2017) suggested in his thesis that current empirical rock mass characterisation methods might be oversimplified, as they

[2] holds for angles between joints of approximately 90°

do not consider spatial discontinuity distribution. He investigated the influence of block shapes, and showed on the one hand an effect on the rock mass stability in terms of instable and kinematical free blocks, and on the other hand an effect onto the rock mass strength in terms of stress distribution.

When characterizing block shapes, Palmström (2001) suggests to distinguish between block shapes formed by regular and irregular joint patterns. Rock masses with a relative regular joint network can be classified into the following block shapes:

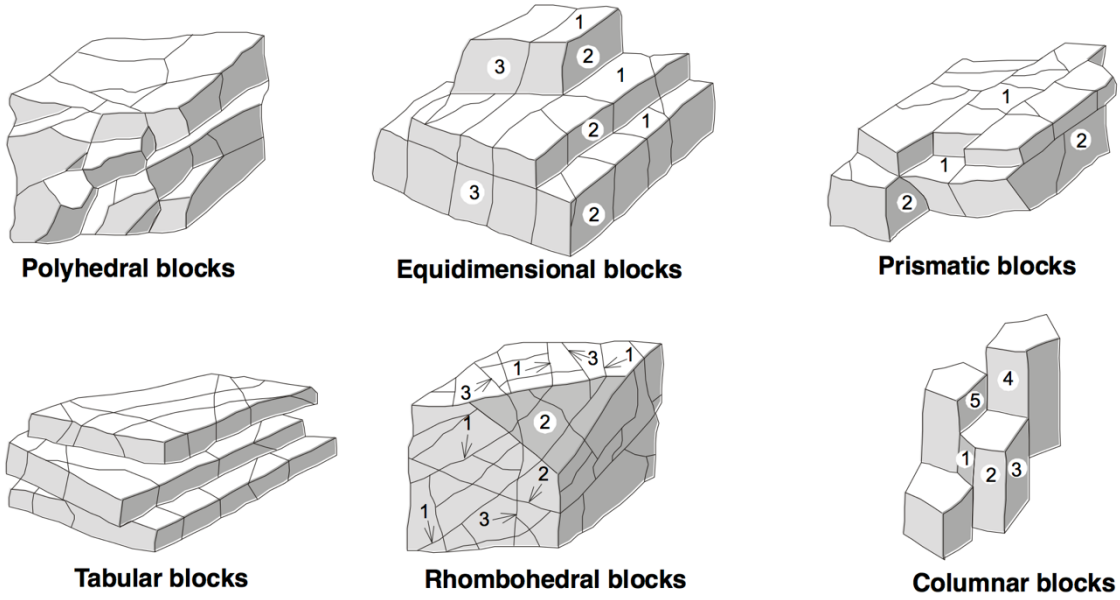

Figure 2.2: Modified examples of block shapes or the jointing pattern (Palmström, 2001).

If no regular joints exist, it is difficult to give an adequate characterization of the jointing pattern. Therefore, a rough estimation of the block shapes according to the following figure is more practical:

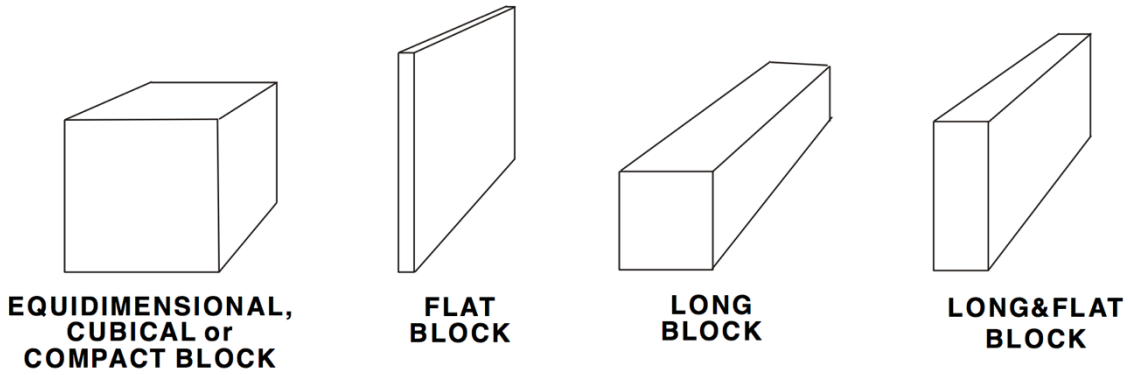

Figure 2.3: Main types of blocks (Palmström, 1995).

Palmström (1995) developed a simplified method for describing blocks with arbitrary polyhedral geometry formed by more than six faces, using the block shape factor β. This factor considers the longest (a_3) and shortest (a_1) dimension of the block (eq. 2.6).

$$\beta = 20 + 7 \cdot \frac{a_3}{a_1}, \tag{2.6}$$

A numerical approach for the determination of block shapes is the block shape characterization method developed by Kalenchuk et al. (2006). It is a spatial mathematical method where two factors, α and β, are used to describe different block shapes. The inter-vertex co-linearity is used to determine whether a block is elongated or not. Therefore, all inter-vertex dimensions (chord lengths) of a block have to be calculated. After that, all chord lengths less than the median length are disregarded as they are not indicative for block shape while long chords and the angular relationships between them can be used for the determination of rod like blocks. Thus, the elongation factor β is described as:

$$\beta = 10 \left[\frac{\sum (a \cdot b)^2}{\sum \|a\|^2 \|b\|^2} \right]^2 \tag{2.7}$$

For elongated shapes, the longest chords are nearly parallel, which results in a maximum β-value of 10, whereas in an equidimensional block all chords are about the same size and orthogonal to each other, which results in a β-value of 0.82. As the β-axis used for the block shape diagram (cf. Figure 2.4) is truncated at a lower bound value of 1, blocks with β-values less than one are plotted on the lower edge. Platy objects return a range of values, as the significant vertex-to-vertex contacts are co-planar. Therefore, for platy blocks the α-value, which considers the surface area to volume ratio, is used and defined as:

$$\alpha = \frac{A_s l_{avg}}{7.7V} \tag{2.8}$$

where $A_s$denotes the surface area, $l_{avg}$the average chord length and V the block volume. The numerical value 7.7 is used for normalization, resulting in an α-value of 1 for a perfectly shaped cubic block, whereas platy blocks return α-values near the maximum of 10. Combining both shape values, block shapes can be visualized using a triangular shaped diagram with almost perfectly shaped cubic, elongated and platy blocks at each corner.

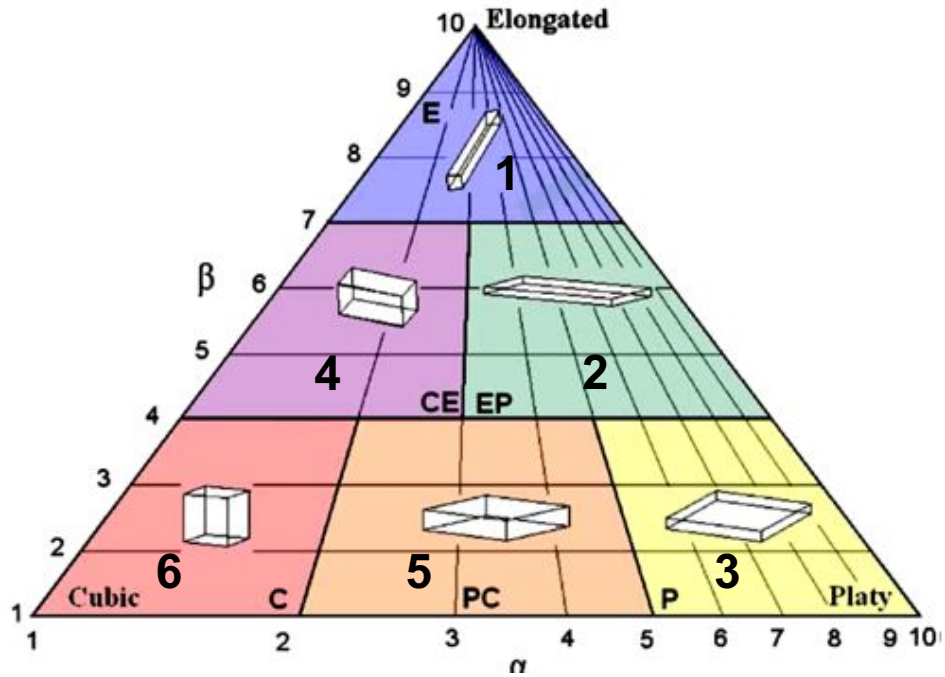

Figure 2.4: Block shape diagram showing zones that encompass basic shapes and the simple sample block (Kalenchuk et al., 2006).

The diagram shown in Figure 2.4 can be used, to visualize the block shape distribution of a jointed rock mass. For a better denotation, numerical values were added to each block shape due to better comparison possibilities.

2.2 Discontinuity controlled block fall and overbreak

According to the Guideline for the Geotechnical Design of Underground Structures with Conventional Excavation (Austrian Society for Geomechanics, 2010), discontinuity controlled block fall (Ground Behaviour Type 2) causes overbreak and is therefore investigated in this thesis. Overbreak can be described as the kinematical process of readjustment of openings due to geological conditions. (Goodman & Shi, 1985). In practice, this means the detachment of single rock blocks into the excavation by either high stresses or an unfavourable joint network geometry, with the excavation forming a kinematically free block.

In underground works, drill and blast is the preferred method for rock excavation. It is used in conventional tunnelling as the first part of a cyclic construction process consisting out of the following three steps:

- excavation using the DBM or other cyclic excavation methods, like mechanical excavators

- mucking
- appropriate support considering the surrounding rockmass

Applying this method, one must consider the damage inflicted to the peripheral rock mass due to high explosive energy, the so called excavation disturbed zone (Fairhurst & Damjanac, 1996). Within the EDZ, additional fractures may promote the kinematical freedom of distinct blocks and hence cause overbreak. Overbreak and discontinuity controlled block fall does not only endanger the safety of the crew, but also increases construction costs and time due to additional material requirement for filling the overbreak. Therefore, a fundamental knowledge of the predominant rock mass and its behaviour as well as required supporting methods after excavation are crucial. In this thesis, a correlation between the joint network, the explosives consumption and the documented overbreak shall be investigated.
The following chapters cover a brief description of this failure mode as well as corresponding supporting measures

2.2.1 Definition

Discontinuity controlled block failure can be best described by the means of block theory (Goodman & Shi, 1985) and wedge theory (E. Hoek, Kaiser, & Bawden, 1995). It is a structurally controlled failure mechanism as a result of an applied force (in most cases due to gravity). Block theory is a globally applied method for the analysis of the kinematic removability/ freedom of potential wedges or blocks due to planes intersecting the excavation surface. Considering the complexity and difficulty of natural blocks being formed by non-persistent discontinuities, some limitations have to be taken into account, expressed by the following assumptions (Goodman & Shi, 1985):

- all joint surfaces are assumed to be perfectly planar (planarity)
- joint surfaces are assumed to extend entirely through the volume of interest (persistence)
- blocks formed by a system of joint faces are assumed to be rigid (deformability)
- the discontinuities and the excavation surfaces are assumed to be invariable as input prameters (consistency)

As mentioned above, a persistence of 100 %, as well as a connected discontinuity set are assumed to form a polyhedron. A connected discontinuity set must feature the following characteristics:

- it is connected to at least two other discontinuity sets
- the intersections of the discontinuity sets must form one connected, finite loop

2.2.2 Support methods

For selecting required bolts or anchors, one must consider the geometry of the wedge as well as the length of a bolt. A schematic of the necessary length of a rock bolt for a given roof wedge, to ensure adequate anchoring is illustrated on the left in Figure 2.5. For roof wedges, the bolt length consists of the length going through the wedge L_w, as well as the length reaching into the intact rock L_R. Experience showed that an anchorage of about 1 meter into the intact rock can be considered sufficient (E. Hoek et al., 1995). Displayed on the right side in Figure 2.5, where there is uncertainty about the dimensions of an instable block, various bolts have to be installed to ensure sufficient anchorage

Figure 2.5: Anchoring of roof wedges modified from E. Hoek et al. (1995).

Summarizing, to design an optimum installation pattern for rock bolts or anchors, one must know about the geometry of the wedges as well as their dimensions. As it is difficult to determine these parameters on site, one should always use a reasonable number and length of anchors, to ensure adequate anchoring.

2.2.3 Kinematic analysis

The kinematical analysis for the determination of potential blocks and wedges is based on the key block theory developed by Goodman & Shi (1985). Two key parameters of the block theory are the finiteness and the kinematic removability of blocks.

The finiteness theorem states that only finite blocks can be subject to movement and instability, indicating that only these blocks merit further analysis. Goodman & Shi (1985) denote a convex block to be finite, if its block pyramid is empty, which implies a convex block to be infinite, if its block pyramid is not empty. An analysis for finiteness of blocks can be done by producing a stereographic projection with given joint planes and free surfaces

The second theorem, denoted as the removability of finite and convex blocks, states that a convex block is removable or not, according to its shape and position to the excavation. Furthermore, the definition of a removable finite, convex block in terms of using stereographic projection is: A convex block is removable, if its block pyramid is empty and its joint pyramid is not empty. A convex block is not removable (tapered), if its block pyramid

is empty and its joint pyramid is also empty (Goodman & Shi, 1985).

Summarizing, the knowledge about the joint network, possible intersections as well as the block geometry and orientation are of importance to determine potential blocks.

3 Methodology

In the following, the methodology to describe the joint network in a DSM with the Software ShapeMetriX^{3D} is presented. The procedure contains a semi-automated identification of joint planes in selected tunnel faces from the Gleinalmtunnel (2nd tube, Styria, Austria, chap. 3.2.1 to 3.2.3) which are consecutively clustered into distinct joint sets with the application SMX Analyst (cap. 3.2.2). The results are on the one side compared to analyses performed with the DSE (Riquelme et al., 2014) and on the other side used to compute the theoretical IBSD and BSD as well as compared to the geological documentation (Geoconsult ZT GmbH, 2015). This analysis is performed with the numerical software 3DEC (Itasca Consulting Group, 2018) according to the approach of Kalenchuk et al. (2006) and Aichinger (2018).Furthermore, the tunnel documentation (Geoconsult ZT GmbH, 2015), is used for the localization of described overbreaks and discontinuity controlled block detachments, as well as the used support and excavation methods. In chapter 3.3, a kinematic analysis, based on key block theory (Goodman & Shi, 1985),is carried out. Using the software VisKBT (Shi., 2017), a detection of potentially instable blocks is possible. In a last step, the compiled data are used to identify possible causes for major overbreak (chapter 3.4). Figure 3.1 shows the whole approach for the determination of causes for overbreak in a flow diagram.

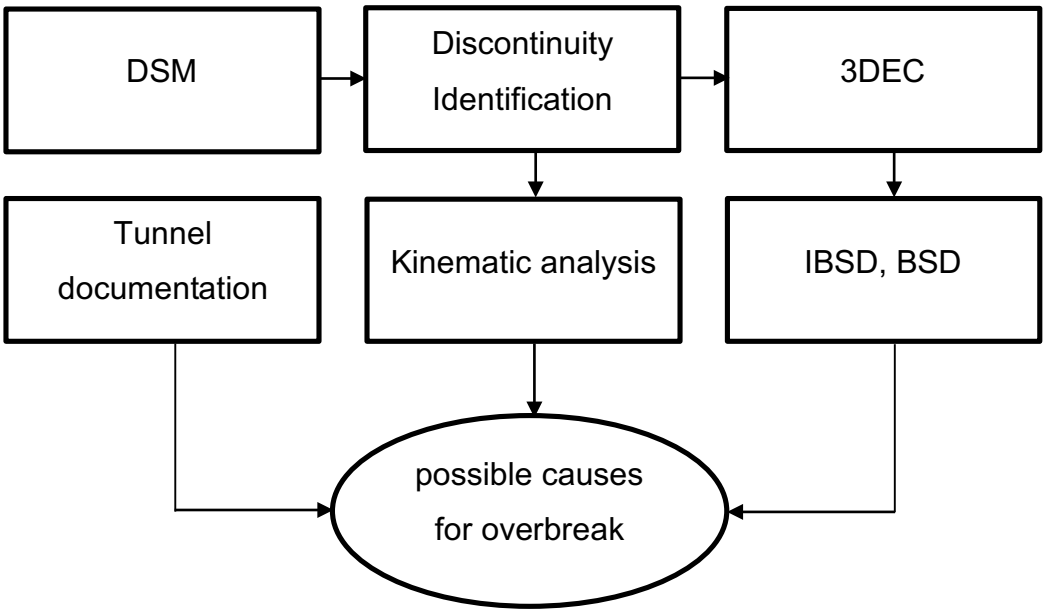

Figure 3.1: Flowchart of the data gathering process for the determination of possible. causes for major overbreak.

3.1 Data basis

As mentioned above, data (Geoconsult ZT GmbH, 2015), which was documented during the excavation of the Gleinalmtunnel, as well as a set of elaborated data regarding the DSE analysis (Buyer et al., 2017) were provided. Consequently, all further analyses in this thesis are based on these data. The documented data include 3D-tunnel face models, the geoloical/geotechnical documentation as well as a list of the excavation progress. The list of the progress is an Excel file containing the amount of explosives used for one blasting round as well as the corresponding support measures for each tunnel section. The data provided by Buyer et al. (2017) included data files which were generated in the process of discontinuity identification using the two applications DSE (Riquelme et al., 2014) and ShapeMetrix^{3D}(3GSM GmbH, 2018), as well as an Excel file containing the corresponding results of the determined DN parameters. A detailed description of the elaborated data can be found in (Buyer et al., 2017).

In a first step, all 3D models were cut, as in the original models, parts of the shotcrete lining were visible, which would have falsified the output (cf. Figure 3.2).

(a) Uncropped 3D model of a tunnel face with visible shotcrete lining.

(b) Cropped 3D model for further analysis.

Figure 3.2: Cropping of a 3D model for a further, objective data processing.

After that, these cut 3D models served as a digital basis for further discontinuity identification analysis including the SMX add on application SMX Analyst (3GSM GmbH, 2018) as well as the DSE (Riquelme, 2016). For the third discontinuity identification method developed by (Andreas Buyer & Schubert, 2018), high resolution pictures of the tunnel faces are necessary to gain representive results. These pictures were also included in the tunnel documentation and therefore used for this method.

3.2 Joint network

The geological documentation (Geoconsult ZT GmbH, 2015) showed that at least the

following three major joint sets dominate the rock mass:

- Foliation (SF): 315 ± 13/ 15 ± 10)
- Joints set 1(SS1): 240 ± 5/75 ± 8
- Tunnel face (SS2): 150 ± 20 / 80 ± 5

The major aim was the detection of these discontinuity sets, and the determination of their corresponding parameters (Set orientation (DD/D), set normal spacing (S), standard deviation of set normal spacing (σ_S), etc.). To obtain the joint set orientations in the DSM, three different approaches were used. The first is based on a method developed by Buyer & Schubert (2017). Therefore, the two applications DSE (Riquelme et al., 2014) and SMX Analyst (3GSM GmbH, 2018) are combined. In a first step, the discontinuity sets are identified using the open source software DSE (Riquelme, 2016), followed by the calculation of the discontinuity set spacing using the multiple scan-line dialog implemented in SMX Analyst. The elaboration of these data (Buyer et al., 2017) was done previously and was kindly provided. The results from DSE were used for validating the second approach.
In the second approach, the different discontinuity sets were identified with a recently developed application in the SMX Analyst, which is described in detail in the following.
The third approach is a pixel-based discontinuity identification based on an optical recognition of joint traces in the digital outcrop images (Buyer, Pischinger & Schubert, 2018; Buyer & Schubert, 2018).
The combination of the results led to an optimum identification of the dominant joint network geometry.

3.2.1 Discontinuity identification with DSE

In a first step, discontinuity stets were identified using the semi-automatic software DSE (Riquelme et al., 2014). This software identifies structural discontinuities in 3D point clouds by clustering planes consisting of points with similar point normal orientations. In a first step, nearest neighbour points are detected, to determine the discontinuity orientation in every point. Afterwards, a determination of principal plane (point with a certain number of coplanar points) orientations is performed. These orientations are compared in a next step to the discontinuity orientations and assigned to common discontinuity sets. A description of the input parameters is listed in Table 3.1.

Table 3.1: Input parameters for the DSE analysis modified from Aichinger (2018), with recommended values (Riquelme et al., 2014).

Parameter	Value	Description
k_{nn}	30	k nearest neighbours. Defines the number of neighbours used to calculate the normal vector of each point.
η_{max}	0.2	Allowable deviation for the co-planarity of points.
n	64	Size of the n by n grid for the KDE.
γ	30	Minimum angle between principal pole normal vectors of discontinuity planes.
N	4	User defined maximum number of discontinuity sets to be detected.
γ_1	30	Maximum angle of surrounding principal poles to be assigned to one discontinuity set.
k	1.5	Cluster distribution threshold for cluster alignment

After that, a visualization of the detected joint sets by assigning different colours was possible. Figure 3.3 shows the point cloud with the by DSE detected joint sets, where each joint set is coloured with different colours. Again, the elaboration of these data was already done and kindly provided (Buyer et al., 2017).

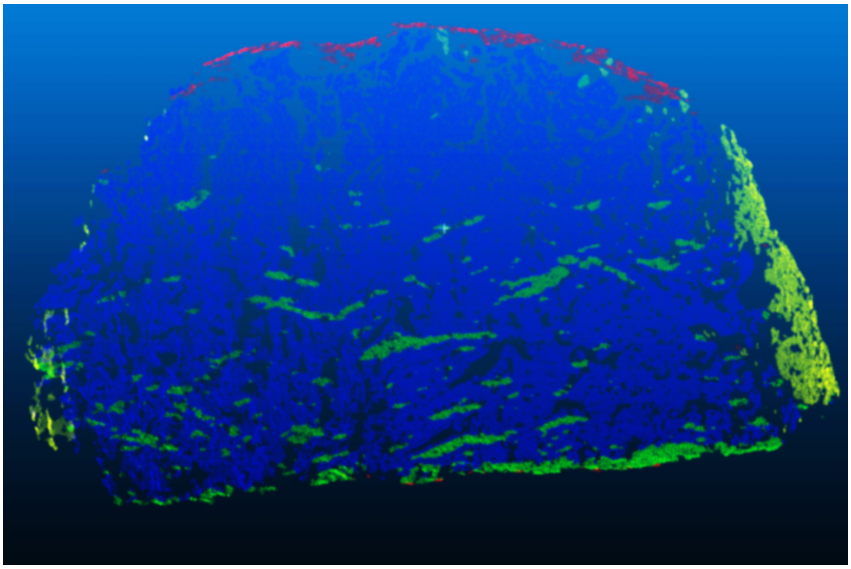

Figure 3.3: Coloured detected joint sets with DSE, depicted in CloudCompare (Girardeau-Montaut, 2018).

3.2.2 Discontinuity identification with SMX Analyst

SMX-Analyst is a software for mapping joint network characteristics like joint planes, traces, rock bridges and water inflow. So far, the single structure elements have to be mapped manually and can be clustered into distinct joint sets via a semi-automated k-means

clustering method. However, in a recently developed add-on, the direct detection of planes in the point cloud is possible. Therefore, an algorithm computes the surface orientations (normal vectors) of the detected joint planes, which are then coloured according to planes with similar orientations. A manual parameter study was performed in order to obtain the best possible results. Aim was the detection of an adequate amount of orientation poles needed to be generated. The parameter study is based on the results from DSE. The following table displays the list of parameters which had to be pre-defined.

Table 3.2: : Parameters for the semi-automatic joint plane detection SMX Analyst.

Parameter	Description
m	the radius for smoothing the orientation measurements of the patches [m]
a_{PP}	The minimum angular deviation between two cluster orientations [°]
r_{PP}	the radius around one cluster centre which the corresponding measurements are assigned to [°]
T_M	A threshold for excluding too weak density distributions [%]
r_c	A curvature radius to define the boundary of a joint plane at a sharp edge [m]
A_{min}	The minimum size of the determined joint planes

For the first computation, a predefined set of values denoted as ‘fine’ was chosen. The output of this evaluation however, gave unsatisfactory results, as the detected number of surface orientations was not sufficient. Consequently, all parameters were continuously refined, until the analysis delivered a result with sufficiently dense and high number of joint planes. An illustration of some tested values as well as the final parameter set (Table 3.3) is given below.

After that, the detected joint planes had to be assigned to their corresponding discontinuity sets via clustering, which is based on and iterative k-means clustering with the following parameters (Table 3.3).

Figure 3.4 shows a comparison of the corresponding computed surface orientations and visualizes the difference of the parameter settings.

Table 3.3: Comparison of different values used for the parameter study.

Parameter	Values for parameter-set 'fine'	Final set of values
m	0.17	0.05
a_{PP}	10	35
r_{PP}	15	40
T_M	1	1
r_c	0.6	0.01
A_{min}	0.5	0.01

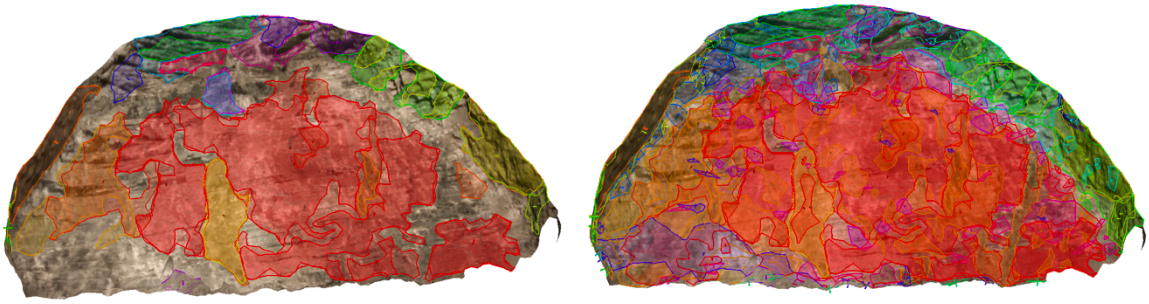

(a) Visualization of the density and amount of detected surface orientations using parameter set 'fine'.

(b) Visualization of the density and amount of detected surface orientations using the finest settings.

Figure 3.4: Comparison of computed number and density of surface orientations with different input values.

Additionally, the option of weighting the joint planes by size was chosen, since the previous joint plane detection allowed for small, insignificant planes to be detected and to ensure plausible results. Concerning the membership angle, adaptions had to be made for each tunnel section, to assure the best possible assignment to the different discontinuity sets. For checking the plausibility of the clustered sets, a comparison of the number of sets with different cluster quality indices was done. The Fukuyama-Sugeno cluster validity index has proven to be the most realistic, and was therefore used for reference.

Table 3.4: Parameters for the joint set clustering in SMX Analyst.

Parameter	Value	Unit
Num. iterations	10	[-]
Membership angle	35-60	[°]
Confidence angle	95	[°]

3.2.3 Discontinuity identification based on digital images

Image-based discontinuity identification was introduced by Franklin et al. (1988) and revised ever since. However, the analyses were mostly restricted in dimension (2D) and the result heavily influenced by light and rock mass conditions. Buyer et al. (2018) developed a method by coupling the 2D restricted, pixel based joint trace detection (JTD) with the 3-dimensional joint plane detection (JPD) and therefore avoids misinterpretations due to falsified pixel data.

In a first step, the original high-resolution images, used for the generation of the DSM, were recovered using the Reconstruction Assistant tool implemented in SMX. In the next step, the region of interest relevant for the analysis, had to be selected (Figure 3.5)

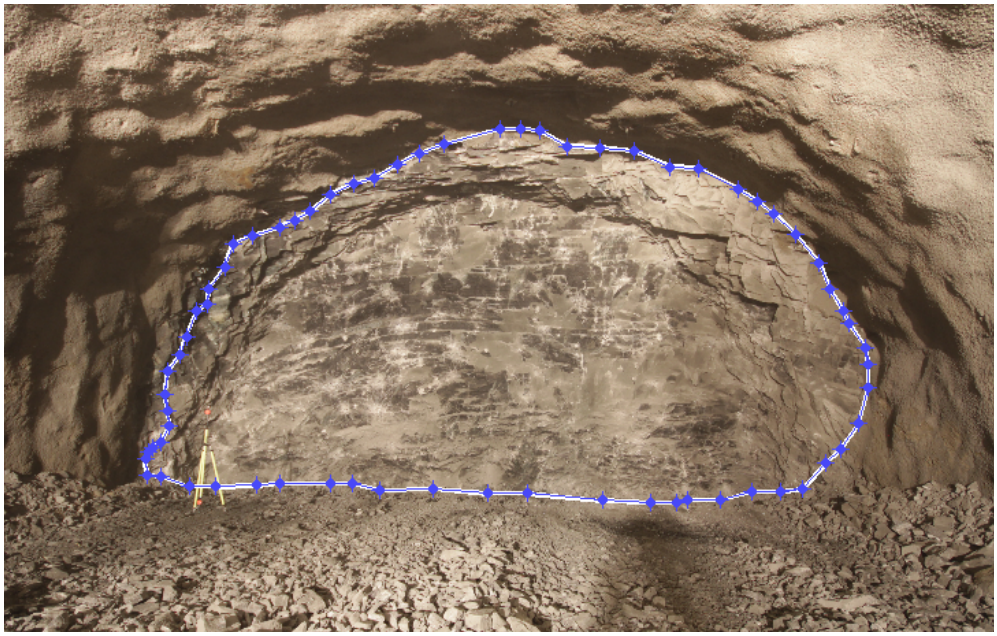

Figure 3.5: Selection of region of interest.

A Matlab-based algorithm then detects edges (using the Canny edge detector), computes their orientation and clusters them according to their dominant 2D orientations. At the end, all orientation clusters are identified, and neighbouring line segments are linked. A detailed description of the process can be found in (Buyer & Schubert, 2018).

After that, a structure map, containing each detected and clustered line segment, is generated. These line segments are considered to be joint traces, and can therefore be analysed using SMX Analyst. All further operations can be done in SMX Analyst as described in chapter 3.2.2.

3.2.4 Determination of the joint normal spacing

The multiple scan-line dialog implemented in SMX Analyst, allows for a determination of spacing parameters, and gives detailed information about the joint traces. Every detected

joint trace is projected on a reference plane, and can be viewed for each joint set individually. However, it does not give any indication regarding the persistence, which is why for all discontinuity sets a persistence of 100 % was assumed. Below, some parameters, that have been analysed and assigned to each set, are listed.
The parameters $\tilde{s}$ and σ_s, listed in Table 3.5, are used for the generation of the 3D model in the following chapter, to determine block size and shape distribution. Due to the more realistic representation of the joint distribution, the median joint spacing was chosen for further analysis.

Table 3.5: Parameters derived with the multiple scan-line tool.

Parameter	Description	Unit
N_i	Number of identified joint traces	[-]
f	Joint set frequency	[1/m]
$\bar{s}$	Mean joint set (normal) spacing	[m]
$\tilde{s}$	Median joint set (normal) spacing	[m]
σ_s	Standard deviation	[m]

3.2.5 Block geometry

The determination of the IBSD and BSD is based on a method developed by Kalenchuk et al. (2006), where the geometry of block shapes is described using shape factors denoted as α and β. Therefore, it was necessary to generate a numerical model for each tunnel section using the 3-dimensional distinct element code 3DEC. The determination of the input parameters of the joint network, in order to generate these 3-dimensional models, was conducted according to chapter 3.2.1-3.2.4. An exemplary list of input parameters for one tunnel section is displayed in Table 3.6.

Table 3.6: Exemplary list of input parameters for the generation of a numerical, 3-dimensional model.

Set ID	DD [°]	D [°]	N_i [-]	$\tilde{s}$ [m]	σ_s [m]	p [-]
SF	337.21	21.71	765	1.91	0.29	1
SS1	348.08	43.76	63	0.09	0.17	1
SS2	245.74	85.07	34	0.05	3.66	1
SS3	142.05	75.90	61	0.10	0.31	1

As every joint set spacing is coupled with a certain standard deviation, it is necessary to run

multiple simulations, to ensure statistically representative results. Therefore, Söllner (2014) performed several replication tests, and proposed 100 replications as a replication factor for each model. However, performing 100 numerical simulations for 23 tunnel sections would have exceeded the time frame of this thesis. Thus, a replication factor of 50 was applied, which is still thought enough to ensure statistically representative results.

3.2.6 Determination of the model size

To ensure a realistic representativeness of the block sizes, an appropriate size of the numerical model has to be evaluated. Kluckner et al. (2015) developed a boundary criterion, where the minimum size of a mapping window is chosen in relation to the average block size. Therefore, it was determined that for each side of the cubic model: $A_{b,mean}/A_{out} \leq 0.001$. This criterion was accomplished by trial and error, where the model size was adapted continuously after each simulation, until the criterion was fulfilled and none of the relevant blocks got intersected by the model boundaries. Hence, each tunnel section was analysed with different, adapted model sizes according to their mean block areas.

3.2.7 Evaluation of ISBD and BSD

Once the numerical models were generated, the IBSD as well as the BSD were determined. Based on the procedure after Kalenchuk et al. (2006), a determination of these distributions was possible. Therefore, the block corners of each block were provided via a 3DEC implemented functionality. After that, the spatial orientation of each block was evaluated. Therefore, the longest corner to corner vertex of each block is identified, and its spatial location within the model, computed. A detailed description of the process can be found in Kalenchuk et al. (2006) and Aichinger (2018).

3.3 Kinematic analysis of the joint network

As mentioned in chapter 2.2.3, the kinematic analysis is based on key block theory developed by Goodman & Shi (1985). Therefore, it is necessary to have sufficient knowledge about the DN forming the blocks. The determination of the joint network was done according to chapter 3.2. After that, a stability analysis could be performed using the analysis software VisKBT (Shi, 2017).

3.3.1 Stability analysis with VisKBT

As mentioned above, for a stability analysis of a jointed rock mass, the joint network and the free faces must be known. An exemplary list of parameters for the stability analysis in is displayed in Table 3.7.

Table 3.7: Parameters for a stability analysation using the KBT based software VisKBT.

Set ID	DD [°]	D [°]	φ [°]
SF	337.21	21.71	20
SS1	348.08	43.76	20
SS2	245.74	85.07	20
SS3	142.05	75.90	20
FF	151.00	90	0

As mentioned in section 2.2.3, a block must have a free face to be kinematically removable. In case of an underground excavation, the tunnel face is considered to be an artificially generated free joint plane, denoted as FF in Table 3.7.
After performing the analyses, the software identifies the blocks and distinguishes between key, potential and stable blocks. As shown in Table 3.8, each block is assigned with a factor of safety and a potential sliding direction described with a normal vector (N_x, N_y, N_z).
After that, the numbers of these different block modes were assigned to each tunnel section in order to generate comparable results.

Table 3.8: Exemplary visualization of parameters derived with kinematic analysis via VisKBT (Shi, 2017).

Planes	Mode	FOS	Sliding direction
0000	Key	0	(0.217, -0.972, -0.0858)
0100	Key	0	(-0.578, -0.366, -0.729)
1000	Key	0	(-0.407, -0.108, -0.907)
0010	Key	0	(0.275, -0.921, -0.276)
1010	Key	0	(0.376, -0.499, -0.781)
0110	Key	0	(-0.0118, -0.864, -0.503)
1110	Key	0	(-0.0844, -0.0867, -0.993)
0001	Stable	1	(0, 0, 0)
1001	Stable	1	(0, 0, 0)
0101	Key	0	(-0.712, 0.647, -0.273)
1101	Key	0	(-0.478, 0.327, -0.815)
0011	Stable	1	(0, 0, 0)
1011	Key	0	(0.326, 0.0625, -0.943)
1111	Key	0	(0, 0, -1)

3.4 Overbreak with respect to the excavation method

The excavation of the investigated 315 m long section of the Gleinalmtunnel was done entirely by DBM. Consequently, the excavation was done in a cyclic advance by blasting the rock mass sections according to predefined dimensions (round length, tunnel face area). However, undesirable overbreaks cannot be avoided and cause additional time and costs. Hence, this chapter deals with the evaluation for causes of this unwanted occurrence.
Each tunnel section was assigned with a series of properties and parameters, which are then put into relation with the degree of overbreak (A/A_D). With A being the surface area of the investigated DSM per round and A_D being the area of the designed cross-section. After that, a correlation study was performed by comparing a set of different parameters, in order to find possible correlations in the different parameters.

3.4.1 Determination of overbreak and possible causes

First of all, a determination of the actual overbreak was carried out. Therefore, the provided data (Buyer et al., 2017), which included the actual blasted tunnel face as well as the volume 1 meter from the tunnel face, were used to determine the over excavation. In a first step, the planned excavation area (A_D) was put into relation with the actual surface area (A), to be able to express overbreak in form of numerical values. However, one must keep in mind that A also includes parts of the roof as well as sidewalls and should therefore always be larger than A_D.
Next, a correlation study was performed using the in Excel implemented CORREL function, which computes, how strongly two variables are related to each other. The equation, used for this function, is as follows

$$Correl(X,Y) = \frac{\sum(x-\bar{x})(y-\bar{y})}{\sqrt{\sum(x-\bar{x})^2 \sum(y-\bar{y})^2}} \tag{3.1}$$

where x and y denote the individual parameter values, and x and $\bar{y}$ their corresponding mean value. Consequently, an output value of -1 indicates a perfect negative correlation, whereas a correlation value of 1 indicates perfect positive correlation. A list of the parameters, used for the correlation analysis, is displayed in Table 3.9. This list contains a mixture of parameters that have been analysed according to the previous chapters, as well as parameter derived from the geological documentation. Values between |0.7 to 1| were seen to indicate a strong correlation, values between |0.5 to 0.7| intermediate correlation and values between |0.4 to 0.5| indicate a weak correlation. Values between 0 and |0.4| were interpreted as non-correlating.
As overbreaks in the geological documentation were classified as minor and major

overbreaks, these descriptions were transformed into comparable values, where 0.5 stands for minor overbreak and a value of 1 for major overbreak. Where there was no overbreak listed, a value of 0.3 was determined.
Another approach for the evaluation of overbreak was, to put the orientation of the main axes of the blocks and their shape in relation to the orientation of the tunnel face, in order to check whether this constellation increases overbreaks at the tunnel face or not.

3.4.1 Excavation and support

As mentioned above, the excavation of the tunnel was done by a cyclic advance. Therefore, different support methods were used to stabilise the rock mass. According to the geological documentation, as a first measure, a shotcrete lining with alternating thickness was applied to the excavated area. In order to gain additional strength, fibre-reinforced concrete was used at selected sections. Additionally, bolts were installed to increase the stability.
After assigning the support measures to each tunnel section, an analysis was carried out by putting the applied support in relation to a various number of different parameters.

Table 3.9: Input parameters for the correlation study.

Parameter	Description	Unit
A_{MAT}	Area of tunnel face calculated from point cloud with Matlab	[m^2]
A_{SMX}	Area of tunnel face calculated DSM with SMX	[m^2]
V	Volume 1 metre from the tunnel face	[m^3]
D_v	Degree of visible drillings on tunnel section expressed by values	[-]
AD	Planned excavation area	[m^2]
A/A_D	Ratio of excavated to planned area	[-]
V/A_D	Ratio of Volume to planned excavation area	[-]
DoF	Degree of fracturing	[-]
UCS	UCS of dominating rock mass	[MPa]
DoO	Degree of overbreak	[-]
Faults	Degree of faults	[-]
VB_{25}	25% quantile of block volume	[m^3]
VB_{50}	50% quantile of block volume	[m^3]
VB_{75}	75% quantile of block volume	[m^3]
V_{min}	Smallest block volume JN	[m^3]
V_{max}	Biggest block volume in JN	[m^3]
A_{bmean}	Average block surface area	[m^3]
V_{bmean}	Mean block volume	[m^3]
BS	Block shape	[-]
N_{tot}	Number of total joint traces detected at on the excavation area	[-]
V/A	Ratio of volume to calculated excavation area	[m^2]
N_{tot}/A	Ratio of total joint traces to calculated excavation area	[$1/m^2$]
E_{OB-1}	Total amount of explosives used for one blasting round	[kg]
$E_{OB-1,s}$	Amount of explosive in relation to the volume, used for one BR	[kg/m^3]
E_{OB+1}	Total amount of explosives used for successive BR	[kg]
$E_{OB+1,s}$	Amount of explosives in relation to V, used for the successive BR	[kg/m^3]
RL	Round Length	[m]
N_{tot}/V	Ratio of total joint traces to calculated volume	[$1/m^3$]
F_{med}	Median frequency of detected joint traces	[1/m]
S_{med}	Median standard deviation of detected joint traces	[m]
N_{kfb}	Number of kinematically free blocks	[-]
Key	Number of key blocks	[-]
Potential	Number of potential blocks	[-]
Anchors	Number of anchors used	[-]

4 Results

This chapter provides an overview of the results elaborated in this thesis. Chapter 4.1.1 displays the results of the DN identification according to the three different approaches described in chapter 3.2.1 to 3.2.3. Moreover, the chosen sets fitting best to the joint sets derived from the geological documentation, are depicted in Table 4.1. Chapter 4.1.3 visualizes the results of the investigation regarding the IBSD as well as the BSD. After that, the result of the kinematic analysis represented by assigning different block modes to each tunnel section is displayed in Table 4.14. Subsequently, the results of the correlation study as well as further approaches for the evaluation of causes for overbreak are shown in chapter 4.3.

4.1 Joint network

4.1.1 Discontinuity identification using 3 different approaches

In order to obtain representable results, three different DN approaches were carried out to find the joint sets formfitting best to the geological documentation. Table 4.1 shows the discontinuity sets according to the geological documentation (Geoconsult ZT GmbH, 2015). As it is not possible to show the results for every tunnel section, tunnel section 2116.60 was chosen for an exemplarily representation of the discontinuity identification.
Table 4.1 displays the joint networks identified manually on site. These joint sets provide the basis for any further analysis, as the aim is to identify them using semi-automatic software approaches. Chapter 4.1.1.1 to 4.1.1.3 display the results using these approaches. Moreover, the joint sets. corresponding the best with the joint sets derived from the geological investigation are highlighted in green. Thus, a visual identification of the approach providing the best correlation with the geological documentation is possible. Where there is no correlation for individual sets, the sets from the geological documentation were used to ensure representative results.

4.1.1.1 Discontinuity identification with DSE

With the input parameters mentioned in chapter 3.2.1 and a maximum number of four detectable joint sets, the results for the chosen tunnel section are shown below.

Table 4.1: JN geometry from the geological documentation (Geoconsult ZT GmbH, 2015).

Section	JS1		JS2		JS3		JS4	
	DD	D	DD	D	DD	D	DD	D
[m]	[°]	[°]	[°]	[°]	[°]	[°]	[°]	[°]
2000.30	330.00	54.00	335.00	70.00	116.00	69.00	84.00	64.00
2009.30	335.00	58.00	305.00	26.00	172.00	83.00	171.00	83.00
2021.30	302.00	88.00	63.00	63.00	58.00	85.00	112.00	73.00
2033.30	341.00	46.00	339.00	39.00	268.00	82.00	86.00	68.00
2046.30	336.00	44.00	340.00	28.00	122.00	75.00	105.00	71.00
2067.80	243.00	79.00	111.00	80.00	359.00	89.00	279.00	80.00
2076.80	344.00	22.00	185.00	83.00	113.00	81.00	123.00	60.00
2088.00	185.00	77.00	190.00	82.00	345.00	29.00	92.00	73.00
2116.60	332.00	38.00	335.00	33.00	230.00	82.00	120.00	69.00
2137.90	358.00	21.00	353.00	81.00	349.00	80.00	141.00	72.00
2148.90	63.00	81.00	97.00	69.00	230.00	60.00	182.00	60.00
2159.20	175.00	75.00	140.00	84.00	274.00	80.00	222.00	50.00
2168.00	356.00	19.00	335.00	32.00	218.00	32.00	274.00	69.00
2185.60	118.00	79.00	141.00	85.00	79.00	83.00	111.00	60.00
2198.80	205.00	63.00	216.00	71.00	271.00	72.00	216.00	71.00
2209.80	323.00	37.00	311.00	15.00	81.00	88.00	321.00	77.00
2240.60	178.00	84.00	171.00	87.00	227.00	75.00	230.00	70.00
2258.20	354.00	19.00	346.00	13.00	118.00	63.00	203.00	51.00
2264.80	324.00	42.00	337.00	37.00	326.00	47.00	242.00	40.00
2280.20	289.00	32.00	294.00	9.00	330.00	52.00	227.00	73.00
2300.00	223.00	46.00	87.00	82.00	262.00	71.00	226.00	53.00
2315.40	255.00	49.00	135.00	89.00	119.00	78.00	196.00	75.00

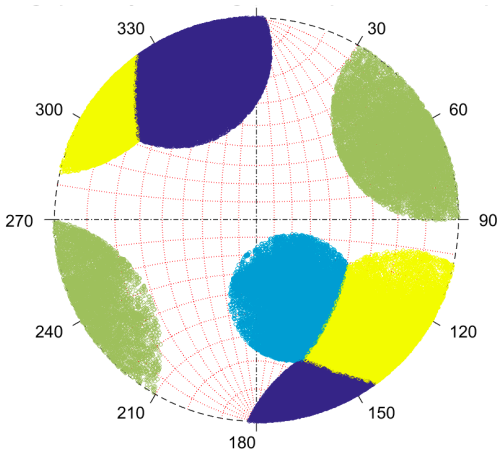

(a) Stereographic projection of detected and assigned principal poles of tunnel section 2116.60.

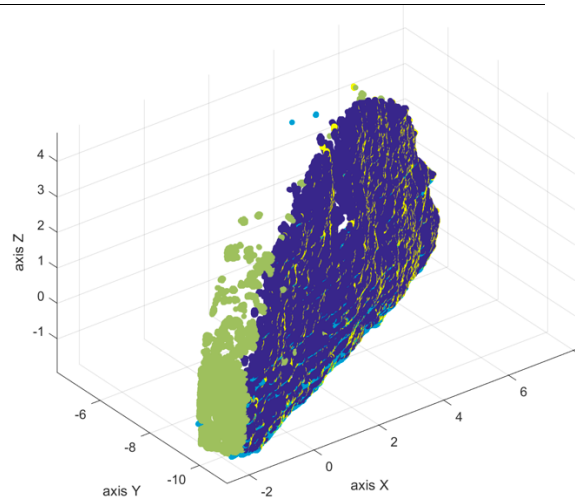

(b) 3-dimensional visualization of detected and assigned principal poles of tunnel section 2116.60.

Figure 4.1: Results of the DSE analysis for tunnel section 2116.60 with assigned principal poles.

Consequently, the following discontinuity sets were identified in section 2116.60 (cf. Table 4.2). A full list of the identified joint set orientations is given in Table 4.3.

Table 4.2: Discontinuity set orientations of tunnel section 2116.60, derived from DSE.

Set ID	DD [°]	D [°]
JS1	335.00	42.99
JS2	154.21	78.68
JS3	131.77	89.40
JS4	240.03	84.33

Table 4.3: Discontinuity sets identified with DSE.

	JS1		JS2		JS3		JS4	
Section [m]	DD [°]	D [°]	DD [°]	D [°]	DD [°]	D [°]	DD [°]	D [°]
2000.30	337.94	58.00	240.87	80.70	114.97	63.45	353.44	14.50
2009.30	334.78	38.29	240.07	14.07	128.83	85.36	58.63	85.87
2021.30	338.05	60.70	230.96	84.51	229.06	43.45	335.19	8.52
2033.30	344.99	58.16	223.14	87.88	304.83	13.51	43.75	45.43
2046.30	334.69	61.38	228.14	65.76	113.42	74.53	301.84	8.21
2067.80	302.45	78.33	250.27	68.96	336.45	15.66	65.15	51.42
2076.80	335.89	44.43	295.23	5.53	114.60	82.77	78.27	50.98
2088.00	237.64	60.57	279.31	10.74	146.16	41.31	32.90	81.77
2116.60	335.00	42.99	240.03	84.33	152.89	76.38	27.94	80.94
2137.90	119.20	28.14	240.27	75.73	154.24	76.68	131.77	89.40
2148.90	333.66	79.14	234.04	36.91	112.23	33.83	18.74	43.90
2159.20	340.21	71.17	237.82	68.25	144.67	57.01	264.00	12.86
2168.00	2.08	23.73	243.21	40.63	148.41	69.79	25.22	71.75
2185.60	304.98	16.53	238.68	59.71	143.99	64.95	168.32	23.64
2198.80	328.84	63.26	222.95	67.07	148.01	73.70	317.61	15.66
2209.80	330.59	61.24	237.52	39.04	124.81	66.27	46.25	49.00
2240.60	22.29	66.82	227.89	30.92	118.56	59.18	62.10	23.12
2258.20	328.17	67.60	234.71	60.10	134.39	65.58	240.01	11.39
2264.80	313.07	10.33	236.08	65.64	134.51	37.60	93.51	77.54
2280.20	340.99	47.34	234.41	62.59	135.84	54.57	239.62	10.38
2300.00	317.51	22.94	237.68	46.81	79.16	70.59	39.23	69.12
2315.40	340.78	78.69	244.78	45.68	130.46	55.20	41.05	19.89

4.1.1.2 Discontinuity identification with SMX Analyst

The pre-settings mentioned in chapter 3.2.2 were used for this investigation to ensure the highest density of detected orientation points. A visualization of the results for one tunnel section is illustrated below.

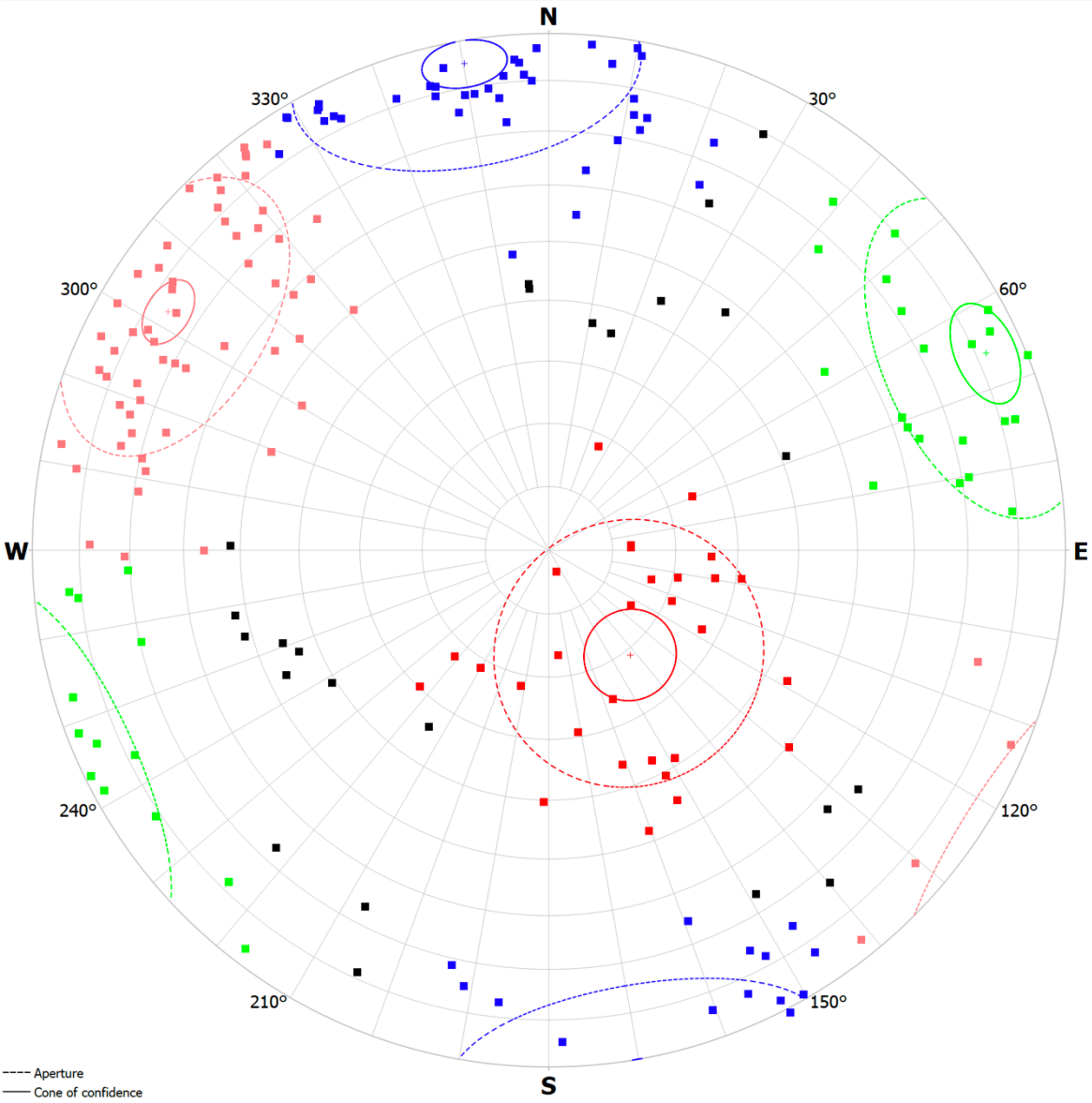

Figure 4.2: Stereographic plot of tunnel section 2116.60 with the plane poles, detected with SMX Analyst, assigned to fitting discontinuity sets. Assigned poles are coloured, whereas black plane poles remain uncoloured, as they couldn´t be assigned to any identified discontinuity set.

Marked with the colours red, green, blue and orange are the assigned plane poles to their corresponding discontinuity sets, whereas uncoloured plane poles remain unassigned. The continuous lines represent a cone of confidence of 95 %, whereas the dashed line displays the aperture of the assigned planes. The membership angle for this tunnel section was set to 50°, as this value provided the best result. For a better visualization of the identified

discontinuity sets, Figure 4.3 displays the corresponding DSM of tunnel section 2116.60 with the assigned and clustered orientation planes.

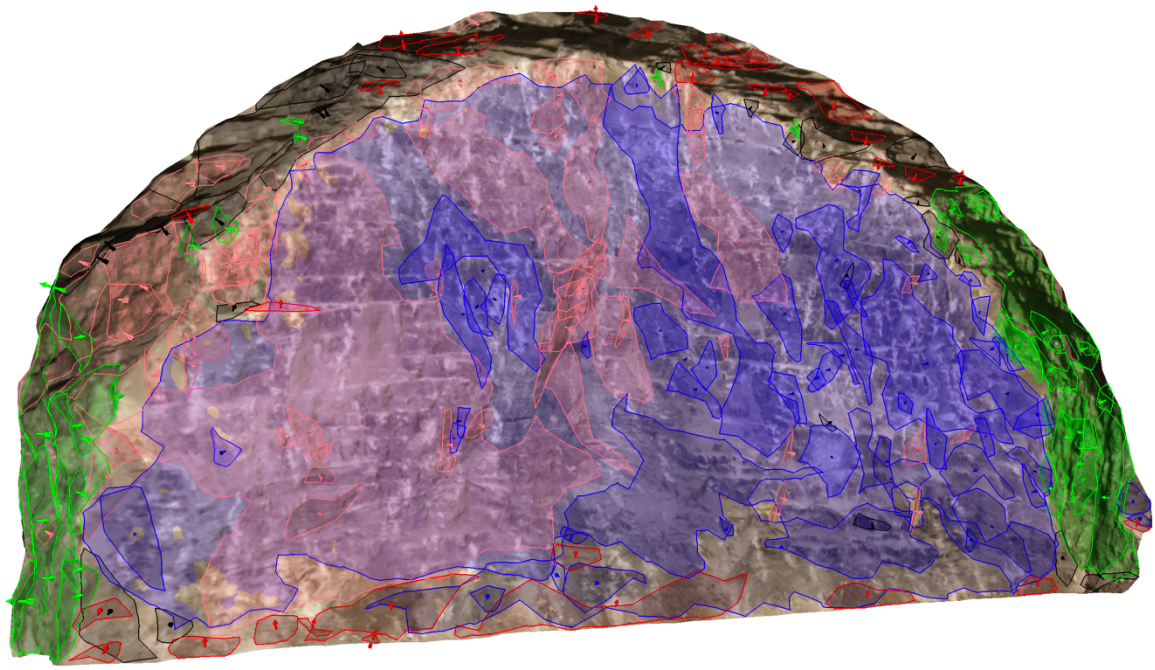

Figure 4.3: DSM showing identified discontinuity sets with clustered orientation planes of tunnel section 2116.60.

Consequently, the following discontinuity sets were identified (cf. Table 4.4).

Table 4.4: Discontinuity set orientations of tunnel section 2116.60, derived from SMX Analyst

Set ID	DD [°]	D [°]
JS1	322.19	20.95
JS2	245.74	82.07
JS3	170.15	85.04
JS4	122.02	75.90

After analysing every specified tunnel section, the identified discontinuity sets were assigned to their corresponding sections and summarised in the following table (Table 4.5):

Table 4.5: Discontinuity sets identified with SMX Analyst for the different tunnel sections.

	JS1		JS2		JS3		JS4	
Section	DD	D	DD	D	DD	D	DD	D
[m]	[°]	[°]	[°]	[°]	[°]	[°]	[°]	[°]
2000.30	335.38	73.11	235.49	76.69	147.12	84.39	59.03	72.00
2009.30	335.36	82.95	242.99	83.00	121.78	83.96	-	-
2021.30	339.08	88.86	-	-	135.99	86.29	57.04	88.29
2033.30	-	-	240.89	79.48	151.12	83.03	28.97	20.68
2046.30	332.65	81.07	232.64	82.38	173.49	72.82	119.77	70.15
2067.80	331.68	81.15	240.81	63.40	130.18	87.33	66.56	87.52
2076.80	331.53	89.31	118.83	79.05	179.00	76.32	59.87	86.80
2088.00	338.03	72.22	234.20	66.16	142.48	72.04	37.54	6.46
2116.60	322.19	20.95	245.74	85.07	170.15	85.04	122.05	75.90
2137.90	328.48	83.61	227.75	67.90	171.54	84.81	106.11	60.62
2148.90	333.70	85.83	231.96	55.67	126.42	74.91	60.11	88.28
2159.20	325.98	74.61	230.12	64.93	166.17	76.04	81.10	43.91
2168.00	314.54	19.15	-	-	150.48	78.82	58.02	88.11
2185.60	340.40	72.27	235.30	72.68	141.93	73.79	-	-
2198.80	330.82	68.38	223.22	55.73	150.21	79.48	62.23	69.80
2209.80	329.33	73.01	208.81	69.57	141.72	67.72	-	-
2240.60	130.54	77.91	244.94	76.70	172.16	84.39	65.50	44.80
2258.20	331.22	62.81	212.68	57.83	142.50	76.36	62.79	58.05
2264.80	180.50	81.57	233.41	58.08	135.82	70.09	57.52	72.37
2280.20	329.50	64.83	215.65	46.68	155.14	76.47	60.61	76.44
2300.00	321.60	70.05	-	-	166.26	69.46	56.23	71.29
2315.40	329.02	55.99	236.58	70.38	155.42	84.84	67.43	51.02

As mentioned in chapter 3.2.2, the membership angle had to be adapted for each tunnel section, in order to obtain the best possible results. Where there are blank cells in Table 4.5, the best result was achieved by clustering three discontinuity sets. The determination of the joint set normal spacing was done according to chapter 3.2.4 and the results are displayed in chapter 4.1.2.

4.1.1.3 Discontinuity identification based on digital images

As mentioned in chapter 3.2.3, an external structure map, according to clustered normal orientations of the patches, was generated for each tunnel section. Consequently, these structure maps had to be imported according to their corresponding tunnel section. Figure 4.4 displays the DSM of tunnel section 2116.60 with its corresponding imported structure map, where detected normal orientations are already clustered and coloured.

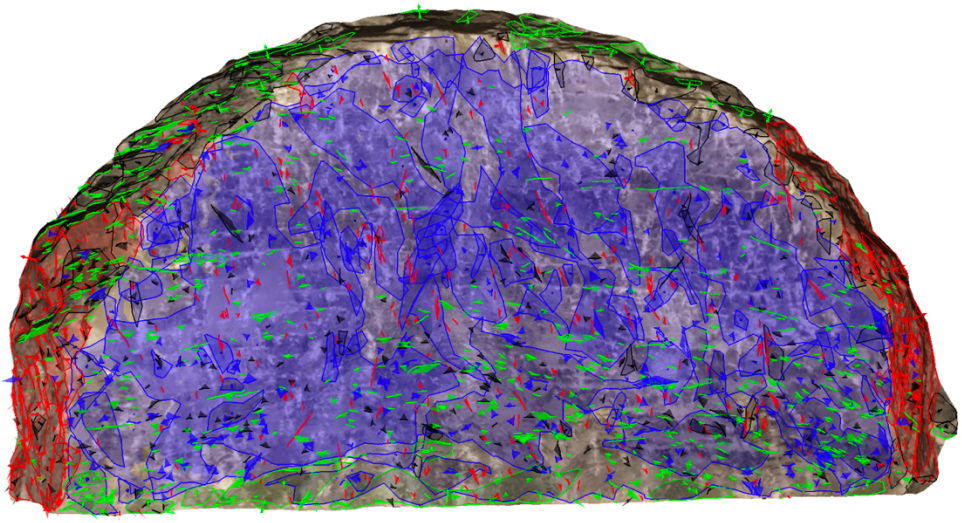

Figure 4.4: DSM of tunnel section 2116.60 with imported JPD and JTD-structure map in SMX Analyst.

Consequently, the stereographic plot of tunnel section 2116.60 depicts as follows:

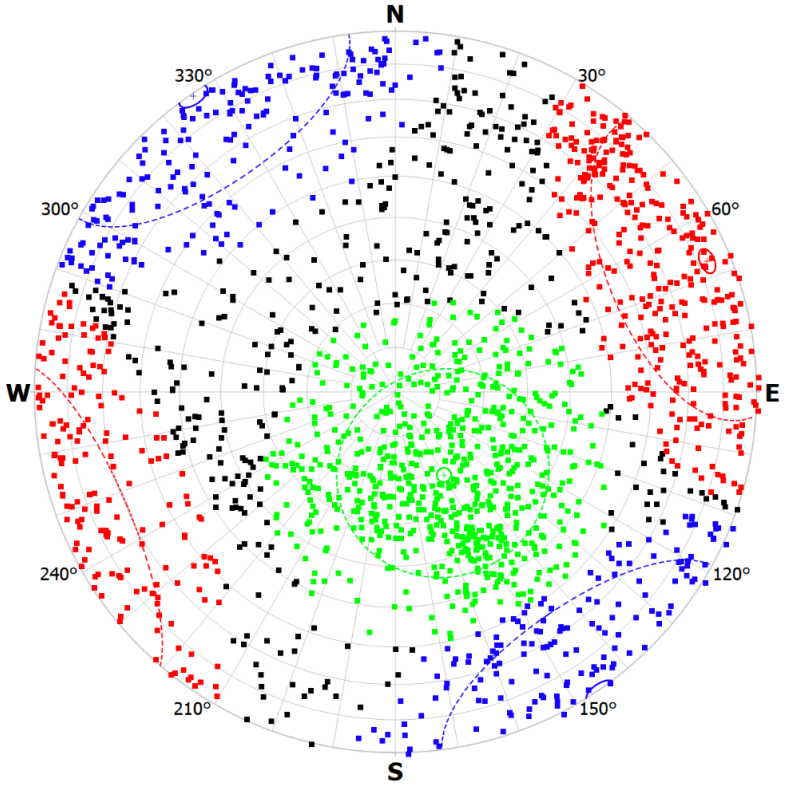

Figure 4.5: Stereographic plot of tunnel section 2116.60 with the plane poles, detected with combined structure maps, assigned to fitting discontinuity sets. Assigned poles are coloured, whereas black plane poles remain uncoloured, as they couldn´t be assigned to any identified discontinuity set.

As visualized in Figure 4.5, the coupling of both structure maps leads to a high additional number and density of detected joint planes. Consequently, the identified joint sets after

clustering, are dominated by the plane poles identified from the JTD. Again, the membership angle was adapted for each tunnel section, in order to obtain the best possible result. Table 4.6 contains the identified discontinuity sets.

Table 4.6: Discontinuity sets identified with combined structure maps.

Set ID	DD [°]	D [°]
JS1	329.79	21.74
JS2	247.21	82.91
JS3	145.67	89.19

Again, every tunnel section was investigated according to this procedure, resulting in Table 4.7. Blank cells in indicate that only three discontinuity sets were identified.

Table 4.7: Discontinuity sets identified with SMX Analyst, based on combined structure maps.

	JS1		JS2		JS3		JS4	
Section [m]	DD [°]	D [°]	DD [°]	D [°]	DD [°]	D [°]	DD [°]	D [°]
2000.30	339.21	28.16	58.06	82.02	156.91	83.82	-	-
2009.30	344.31	16.14	243.19	87.91	340.90	87.69	-	-
2021.30	339.08	88.86	-	-	135.99	81.00	57.04	88.29
2033.30	345.71	9.92	227.77	86.31	135.70	52.10	328.88	56.99
2046.30	338.73	27.84	22.69	79.75	155.05	89.50	135.37	7.19
2067.80	348.35	19.28	248.53	85.83	153.20	16.97	335.30	51.14
2076.80	344.94	18.46	333.99	78.19	71.63	87.33	-	-
2088.00	348.16	21.56	-	-	331.83	83.12	88.12	87.66
2116.60	329.79	21.74	247.21	82.91	145.67	89.19	-	-
2137.90	339.94	16.55	258.29	86.67	158.90	85.78	-	-
2148.90	331.49	29.94	201.25	5.72	161.12	86.22	49.99	83.28
2159.20	326.95	25.33	267.89	77.32	152.58	86.58	154.14	10.50
2168.00	329.11	33.27	59.94	89.98	118.07	89.16	100.65	4.96
2185.60	317.20	14.93	76.98	87.08	313.93	89.04	-	-
2198.80	298.67	5.99	236.47	78.68	335.98	86.98	-	-
2209.80	311.32	10.16	239.23	82.90	328.84	76.44	-	-
2240.60	300.39	11.07	232.87	79.00	313.20	84.10	-	-
2258.20	315.86	17.28	239.37	73.04	319.00	73.03	-	-
2264.80	298.40	10.07	230.93	76.67	315.87	57.71	-	-
2280.20	303.56	30.58	248.53	79.39	151.17	83.09	-	-
2300.00	313.14	18.13	224.24	83.05	329.99	88.36	-	-
2315.40	321.79	17.27	246.01	81.91	150.10	86.11	-	-

4.1.2 Determination of joint network normal spacing

The procedure for the determination of joint normal spacing was the same for each approach. Table 4.8, Table 4.9 and Table 4.10 display the results of the discontinuity identification with the multiple scan-line dialog implemented in SMX Analyst for tunnel section 2116.60. For the joint normal spacing S_{JS}, the median values have been chosen. Due to that it is possible to obtain negative spacing when applying standard deviations. The reason for that is, that joint normal spacing in general shows a distribution skewed to the left, whereas standard deviations are linked to an even Gauß-normal distribution. Therefore, it is possible to obtain a higher standard deviation than spacing.

Table 4.8:Joint set normal spacing for tunnel section 2116.60 based on DSE identification.

	N_{JS}	F_{JS}	S_{JS}	σS_{JS}
JS1	63.00	6.92	0.09	0.17
JS2	184.00	2.25	0.28	0.46
JS3	60.00	0.30	0.14	4.71
JS4	288.00	2.56	0.20	0.52

Table 4.9: Joint set normal spacing for tunnel section 2116.60 based on SMX-Analyst discontinuity set identification.

	N_{JS}	F_{JS}	S_{JS}	SS_{JS}
JS1	29.00	0.37	2.65	2.42
JS2	34.00	0.64	0.05	3.66
JS3	54.00	2.95	0.14	0.47
JS4	61.00	4.27	0.10	0.31

Table 4.10: Joint set normal spacing for tunnel section 2116.60 based on image-based identification.

	N_{JS}	F_{JS}	S_{JS}	σS_{JS}
JS1	765.00	1.91	0.29	0.65
JS2	416.00	0.89	0.63	1.30
JS3	398.00	0.58	1.19	1.63

A full list of the DN determined with these approaches as well as a comparison with the sets derived from the geological documentation (Geoconsult ZT GmbH, 2015) can be found in the digital Appendix.

4.1.3 Block geometry

As mentioned in chapter 3.2.7, the numerical models were generated with 3DEC, using a replication factor of 50. Furthermore, the model size was adapted for each block surface, to be at least 1000 times the mean block area, to ensure representative results. Additionally, a persistence of 100 % was assumed as to ensure equal boundary conditions regarding the kinematic analysis. In the following, the results of the block geometry for are delineated by means of three different plots. For illustration purposes tunnel section 2000.30 was chosen. Figure 4.6 shows the block volume distribution of 50 replications with the cumulative relative frequency of block volumes in % on the ordinate axis and the logarithmic block volumes on the abscissa. The corresponding quantile values are listed in Table 4.11.

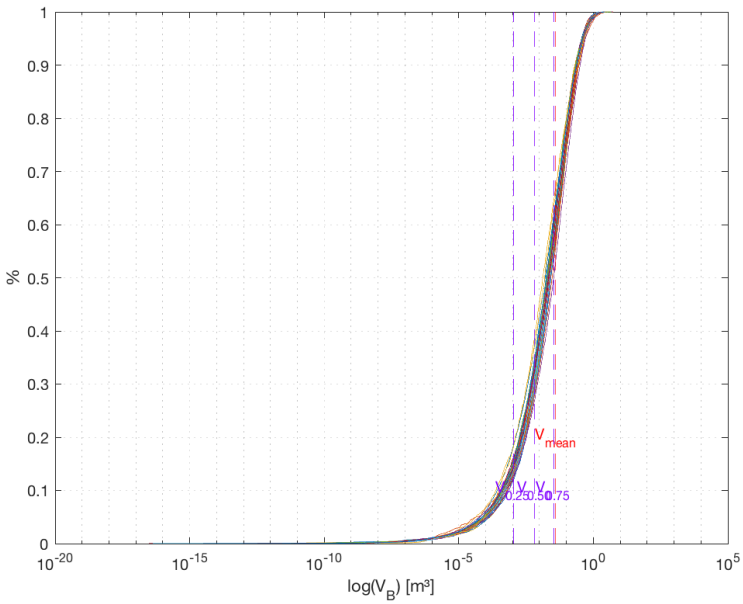

Figure 4.6: Cumulative block volume distribution of 50 replications for tunnel section 2000.30 with corresponding quantile volumes indicated.

Table 4.11: Calculated values of the quantile volumes for tunnel section 2300.30.

Quantile volume	Value	Unit
V_{25}	$3.89*10^{-3}$	[m^3]
V_{50}	$2.26*10^{-2}$	[m^3]
V_{75}	$9.02*10^{-2}$	[m^3]
V_{mean}	$9.12*10^{-2}$	[m^3]

As displayed in Figure 4.6, a relation of $A_{b,mean}/A_{out} \leq 0.001$ delivers block volume distributions with just slight deviations. Figure 4.7 depicts the corresponding block shape distribution in a triangular plot, where the top corner represents elongated blocks, the

bottom left corner cubic blocks, and the right corner platy ones. Moreover, Figure 4.8 illustrates the block orientations by means of the longest corner to corner vertex of each block.

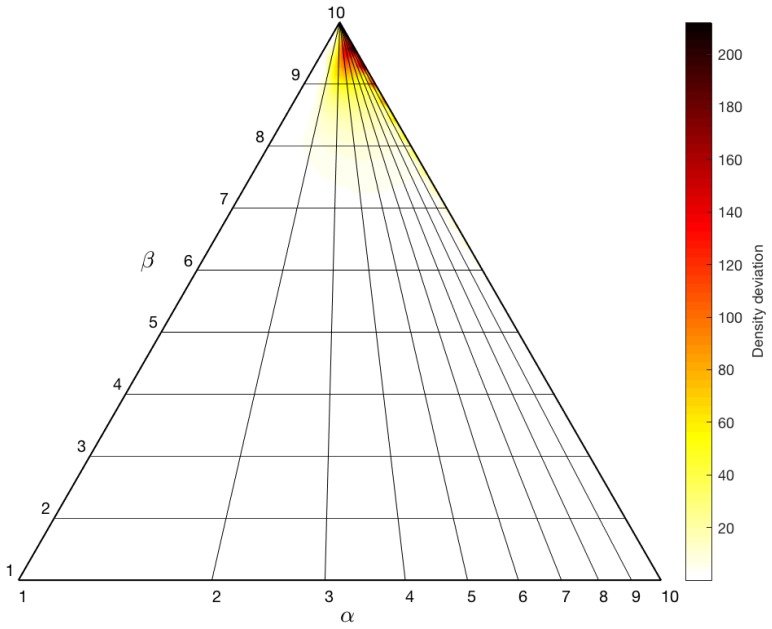

Figure 4.7: Density plot of the block shape distribution of tunnel section 2000.30, indicating very elongated blocks.

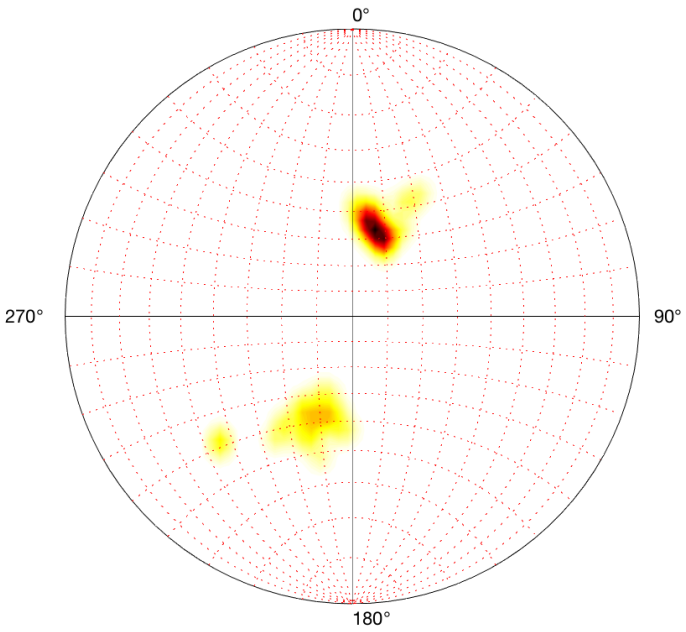

Figure 4.8: Density plot of the block shape orientations, with respect to the longest corner to corner vertex, of tunnel section 2000.30.

As visualized in Figure 4.8, two peaks are depicted, where the second one is rotated by 180°. The reason for this is that there might be several long vertices occurring in one block pointing into opposite directions, which cause these peaks.

4.1.3.1 Block volumes

In the following, the results of the block volume determination are summarised. In Table 4.12, the determined block volume quantiles for each tunnel section are listed. The computed median mean block volume for all tunnel sections is 0.601 ± 0.42 m^3.

Table 4.12: Quantile-and mean volumes along the investigated tunnel sections.

Section [m]	V_{25} [m^3]	V_{50} [m^3]	V_{75} [m^3]	$\overline{V_{b,mean}}$ [m^3]
2000.30	3.89E-03	2.26E-02	9.02E-02	1.02E+00
2009.30	2.89E-03	1.99E-02	8.98E-02	1.16E+00
2021.30	2.90E-03	2.00E-02	9.08E-02	1.17E+00
2033.30	6.34E-04	3.56E-03	1.41E-02	2.99E-01
2046.30	7.24E-04	4.78E-03	2.08E-02	4.02E-01
2067.80	1.83E-03	7.85E-03	2.56E-02	9.84E-01
2076.80	8.23E-03	3.38E-02	9.40E-02	1.08E+00
2088.00	1.47E-03	7.64E-03	2.84E-02	4.19E-01
2116.60	1.55E-05	8.46E-05	3.40E-04	1.90E-02
2137.90	2.07E-03	1.21E-02	4.89E-02	1.05E+00
2148.90	6.75E-05	3.19E-04	1.15E-03	7.79E-02
2159.20	1.44E-03	8.50E-03	3.56E-02	9.12E-01
2168.00	5.21E-04	2.68E-03	1.05E-02	2.44E-01
2185.60	1.33E-03	9.20E-03	4.23E-02	6.91E-01
2198.80	1.29E-03	7.69E-03	3.22E-02	7.94E-01
2209.80	1.10E-03	5.92E-03	2.36E-02	3.66E-01
2240.60	3.28E-03	1.78E-02	6.80E-02	1.41E+00
2258.20	1.46E-03	8.17E-03	3.36E-02	5.12E-01
2264.80	1.51E-04	8.96E-04	3.70E-03	1.06E-01
2280.20	3.42E-04	2.05E-03	8.69E-03	2.35E-01
2300.00	4.07E-03	2.22E-02	8.47E-02	1.03E+00
2315.40	6.83E-05	4.22E-04	1.85E-03	6.76E-02

4.1.3.2 Block shapes

The distribution of the block shapes along the tunnel sections is illustrated in Figure 4.9. Different block forms are distinguished according to their α-and β-values and are described starting from very long, elongated to very flat and platy.

4.1.3.3 Block orientations

Table 4.13 displays the approximate block orientations according to their longest corner to corner vertex and the angle between the block axes and the tunnel axis (151/00).

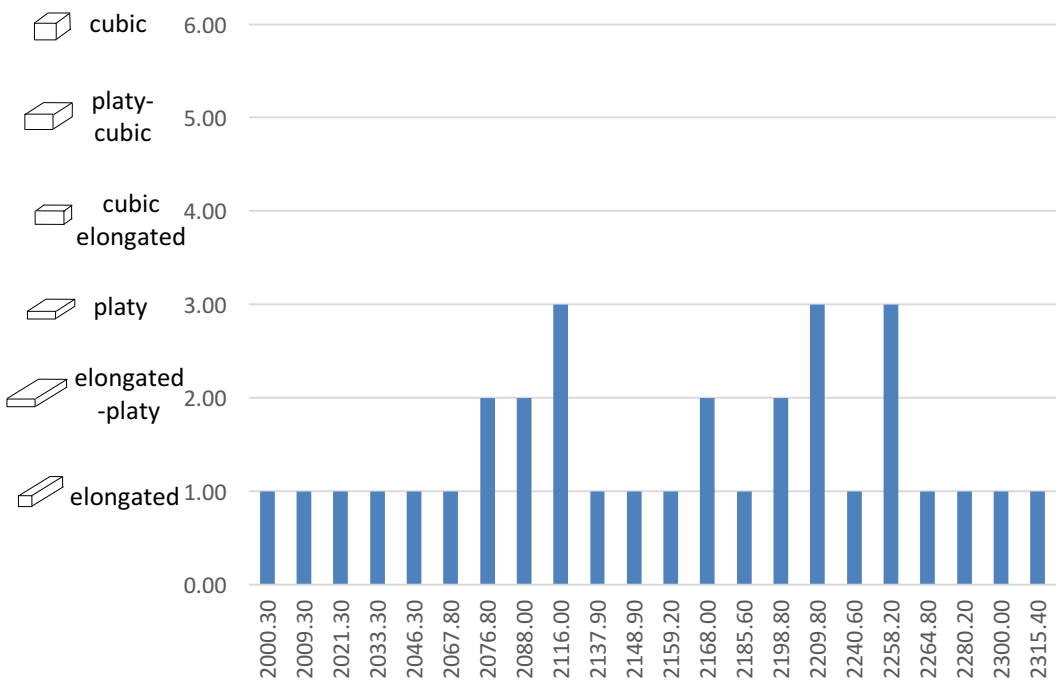

Figure 4.9: Dominant block shapes along the investigated tunnel sections.

Table 4.13: Calculated longest vertex to vertex block orientations for each tunnel section with their corresponding deviations to the tunnel axis.

Section [m]	DD [°]	D [°]	ΔDD [°]	ΔD [°]
2000.30	55	85	96	-85
2009.30	40	20	111	-20
2021.30	40	20	111	-20
2033.30	140	25	11	-25
2046.30	35	30	116	-30
2067.80	160	80	-9	-80
2076.80	50	50	101	-50
2088.00	60	20	91	-20
2116.00	130	50	21	-50
2137.90	60	5	91	-5
2148.90	150	10	1	-10
2159.20	65	65	86	-65
2168.00	0	5	151	-5
2185.60	120	65	31	-65
2198.80	85	65	66	-65
2209.80	115	30	36	-30
2240.60	65	70	86	-70
2258.20	290	10	-139	-10
2264.80	115	30	36	-30
2280.20	100	10	51	-10
2300.00	160	10	-9	-10
2315.40	45	50	106	-50

4.2 Kinematic analysis of joint network

A kinematic analysis was performed using the block theory based software VisKBT (Shi, 2017), in order to determine the number of stable, potential and key blocks. The results for each tunnel section are listed in Table 4.14.

Table 4.14: Determined number of potential, stable and key blocks assigned to each tunnel section.

	Kinematic Analysis		
TS	Key	Stable	Potential
2000.30	8	3	3
2009.30	4	3	7
2021.30	9	3	2
2033.30	6	3	5
2046.30	4	3	7
2067.80	9	3	2
2076.80	6	3	5
2088.00	7	3	4
2116.00	6	3	5
2137.90	4	3	7
2148.90	10	3	1
2159.20	10	3	1
2168.00	4	3	7
2185.60	10	3	1
2198.80	6	3	5
2209.80	7	3	4
2240.60	10	3	1
2258.20	7	3	4
2264.80	5	3	6
2280.20	4	3	7
2300.00	6	3	5
2315.40	8	3	3

4.3 Overbreak with respect to the excavation method

This chapter shows the result of the correlation study in order to determine causes for overbreak. Therefore, parameters that correlate with the ratio of $\mathrm{A/AD}$ and recorded values of major overbreak derived from the geological documentation, were determined. A full matrix of the correlation study, where correlation values lower than -0.5 and higher 0.5 are highlighted in green, can be found in Appendix A.

4.3.1 Determination of overbreak

The result of the correlation study for the listed overbreak of the geological documentation showed correlations between the mean block volume V_{bmean}, as well as the used amount of explosive E_{OB-1}. Plots of the determined correlations in relation to the tunnel sections are depicted in Figure 4.10 and Figure 4.11. The correlation study between the mean block volume and overbreak resulted in a positive correlation value of 0.51, which is visually depicted in Figure 4.10. Additionally, a polyline visualizes a similar curve progression and therefore correlation.

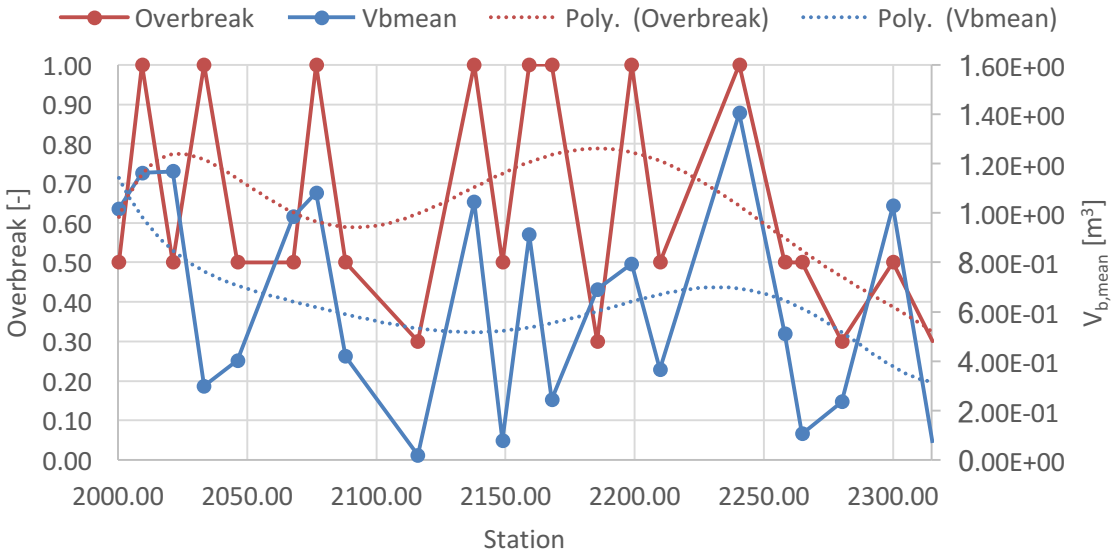

Figure 4.10: Positive correlation between mean block volume V_{bmean} and documented overbreak.

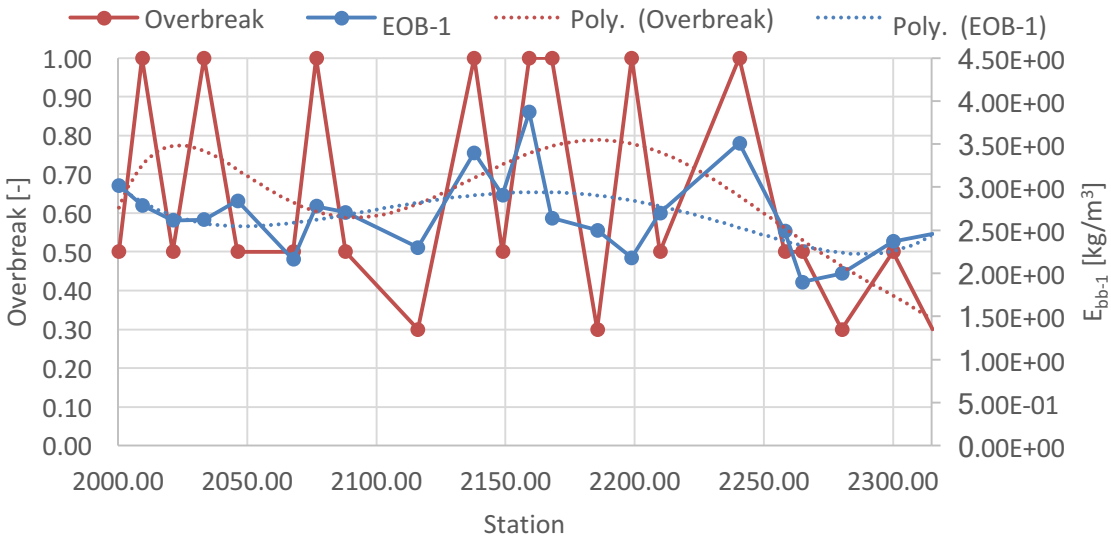

Figure 4.11: Positive correlation between used amount of explosives with regard to the volume and documented overbreak.

The correlation matrix resulted in a positive correlation value of 0.53, which is depicted in Figure 4.11. Further correlations investigated are parameters correlating with the ratio of excavated area to the planned excavation area A/AD. As a result, the correlation matrix showed good correlation to the round lengths.

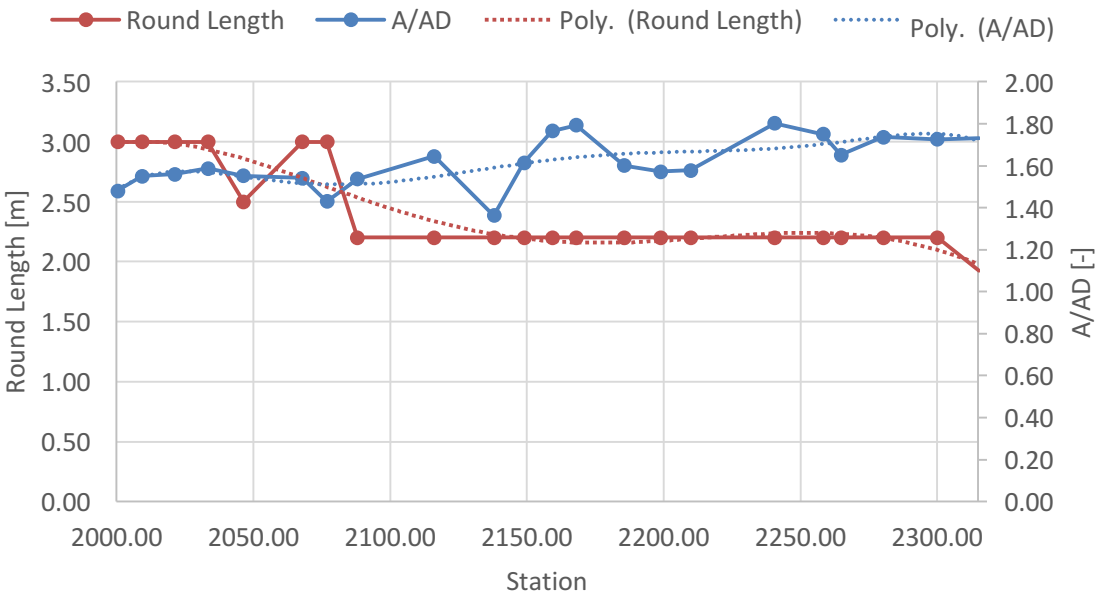

Figure 4.12: Negative correlation between round length and ratio of planned and excavated tunnel face areas.

Figure 4.12 depicts the correlation between the round length and A/AD with a negative correlation value of -0.53.

4.3.2 Excavation and support

The correlation study showed no significant correlations between excavation and support and is therefore not investigated further.

5 Discussion and Interpretation

In the following, a comparison between the three different discontinuity identification methods, as well as an evaluation of the method that delivered the most realistic results (compared to the geological documentation), is done. Next, the results of the kinematic analysis are discussed, and possible correlations with overbreak investigated. Chapter 5.3 addresses the results gained from the correlation study and debates their outcome.

5.1 Determination of rock mass geometry

For the rock mass geometry, aim was to detect at least the discontinuity sets, which were also identified by the geologists on-site, in order to find their true set normal spacing. Chapter 5.1.1 discusses the different discontinuity identification methods and the number of sets, that were chosen from each method for further investigation. The next section deals with the dominating block geometry, which was determined for each tunnel section in a subsequent step.

5.1.1 Joint network

The rock mass along the investigated section is dominated by the three major joint sets, described in chapter 3.2. Analysing the results, no clear statement can be made, which identification method delivered the most realistic results. The identification method using the DSE, provided 26 matching discontinuity sets, the SMX Analyst method 28, and the image-based method 20. Hence, neither of the applied methods on its own provided a good overall-correlation with the measured discontinuity sets from the geological documentation. Nevertheless, individual identification methods seem to detect certain discontinuities, that others were unable to. The image-based method for example seemed to detect the foliation in almost every section, whereas the SMX Analyst method could not detect it at all. The DSE managed to detect the foliation in some sections, but didn´t in others. However, by combining the three methods, most of the discontinuity sets could be identified with just slight deviations of ± 12° for dip direction and ± 8° for dip angle. Comparing the set normal spacing of the detected and documented joint sets, a good correlation can be determined, with the dominant joint spacing being between 6 and 20 cm (Figure 5.1).

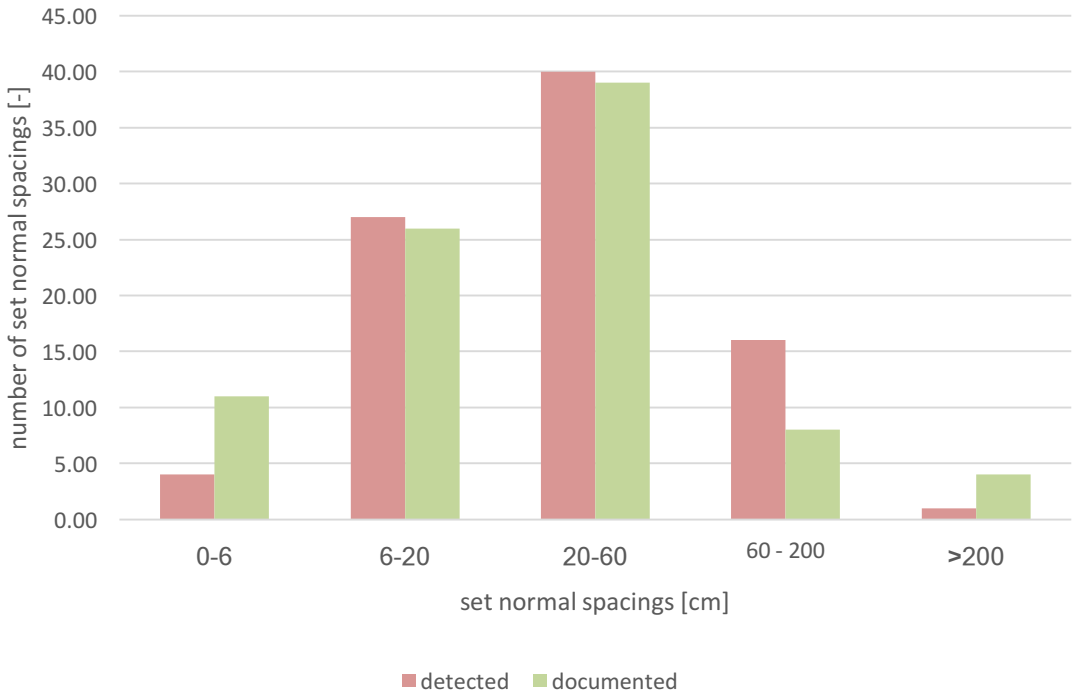

Figure 5.1: Comparison of detected and documented set normal spacing.

As illustrated in Figure 5.1, slight deviations occur at very small and a very large joint set spacing. The reason for that is, that in the geological documentation, some faults are described to have zero joint spacing, whereas others were assigned with a joint spacing higher than 2 m. As remote sensing techniques can only detect visible joint planes, it is not possible to identify faults containing cataclastic material, since both vector-based approaches (DSE/SMX), identify joint planes based on the DSM. Therefore, it is necessary to have clearly distinguishable planes of a certain size (depending on the resolution of the DSM) consisting of either points with subparallel normal vectors (DSE) or co planar mesh patches (SMX). However, as faults tend to show no consistent jointing pattern, no similar oriented planes respectively points can be detected and assigned. Moreover, discontinuity sets with a joint normal spacing larger than two meters could not be identified as such, as the distance, in relation to the investigated area (i.e. tunnel face), is too big. Consequently, too few joint traces were detected, not allowing clustering them and assign an entire discontinuity set. However, a direct comparison between the spacings of the documented and identified joint sets, shows a recognisable deviation, as only 47 of the 88 joint spacings are in accordance. A general underestimation of the manually mapped joint spacings in relation to the detected ones could be obtained. This leads to the assumption, that either the manual on site assessments, or the remote sensing approaches used in this thesis, have not delivered an accurate description of the actual existing joint network.

5.1.2 Block Geometry

As the block volume and shape determination of blocks in a DN is a theoretical approach, using the information about the set normal spacing and its standard deviation of the previously identified joint sets, the outcome of this investigation can only be considered as an estimation.

5.1.2.1 Block volume

For the block volumes, a replication factor of 50 in combination with the criterion $A_{b,mean}/A_{out} \leq 0.001$ delivered good results, with only slight deviations between single simulations (cf. Figure 4.6). As a result, mean block sizes ranging from 0.00116 – 0.0987 m^3 were determined (cf. Figure 5.3). As the dominating set normal spacing ranges from 2 to 60 cm, these volumes can be considered as plausible results. According to EN ISO 14689-1 (2016), these block sizes are from a small to a moderate size. (cf. Table 2.2).

5.1.2.2 Block shape

According to Figure 4.9, the block geometry is dominated by elongated blocks. Only seven out of the 22 investigated tunnel sections show a tendency to platy block shapes. The block shape is controlled by the very thin layered foliation and the other two wider spaced joint sets.

5.1.3 Block orientation

When analysing the block orientation, one must keep in mind that this orientation is calculated from the longest vertex to vertex distance of each block. Consequently, results of this study only give just a rough estimation of the actual spatial block location. For very elongated blocks on the other hand, the calculated orientation is realistic, as there is good accordance of the orientations between its longest edge and longest vertex. By analysing Table 4.13, a slight tendency of the block orientations to the foliation, which is orientated 315 ± 13/ 15 ± 10, is noticeable. As mentioned in chapter 4.1.3, one must consider that blocks, which are oriented the opposite dip direction, are still considered to be dominated by the foliation.

5.2 Kinematic analysis of joint network

Analysing the results of the kinematic analysis (cf. Table 4.14), it is obvious that 14 block behaviour modes (key, potential and stable) are generated by the intersection of 4 joint sets.

Moreover, this constellation of 4 joint sets, always develops 3 stable blocks, and a varying number of key and potential blocks. After examining the relation and influence of these kinematic modes with the documented overbreak, a shifted negative correlation of -0.66 with potential blocks, respectively a shifted positive correlation of 0.66 with key blocks, is visible in Figure 5.2.

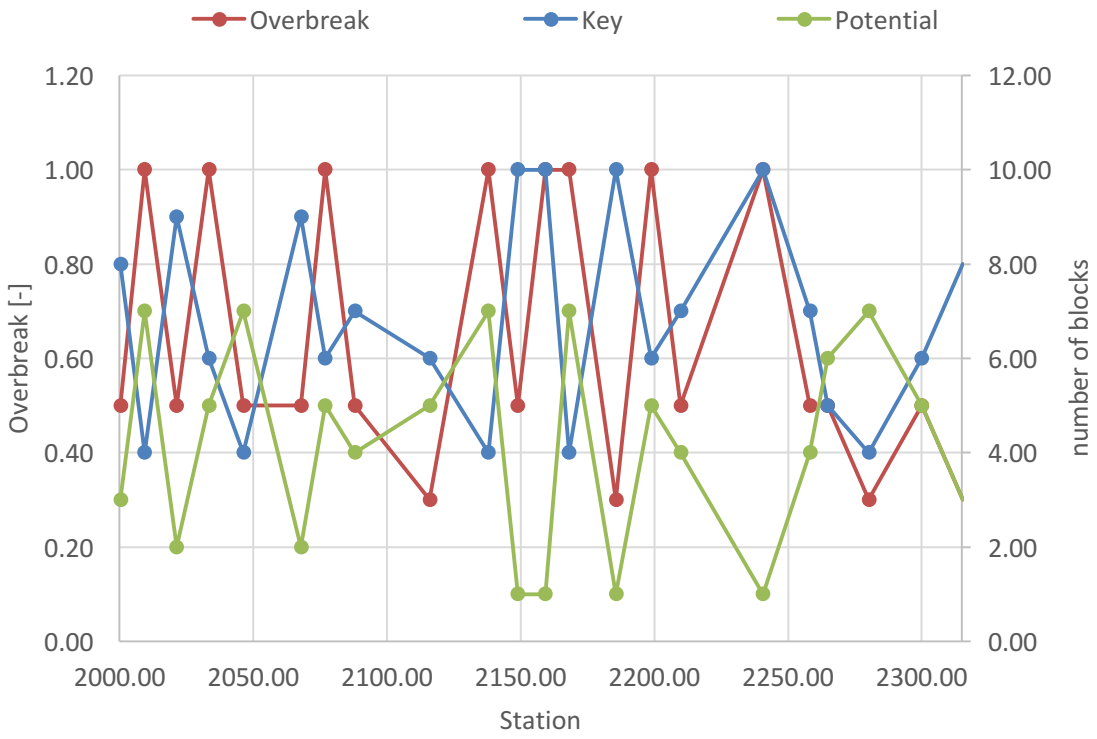

Figure 5.2: Comparison of kinematic modes with documented overbreak.

Hence, the assumption can be made, that an increasing number of key blocks might be an indicator for overbreak in advance.

5.3 Overbreak with respect to the excavation method

As mentioned in chapter 4.3, significant factors for overbreak are on the one hand the amount of explosives in kg/m^3, used for one blasting round, as well as the block geometry. By analysing Figure 4.11, one can assume that amount of explosives from around 2.5 kg/m^3 led to major overbreak in almost every investigated tunnel section, whereas amounts below this value resulted in minor overbreak if any at all. This suggests the assumption that an “overloading” of the boreholes can lead to major overbreak at the investigated tunnel sections, since the depth of the excavation disturbed zone reaches deeper into the rock mass. Furthermore, the determined mean and quantile values of the IBSD indicate some correlation with overbreak as well. Figure 5.3 illustrates a comparison of the theoretical

block geometry (IBSD and BSD) with the documented overbreak.

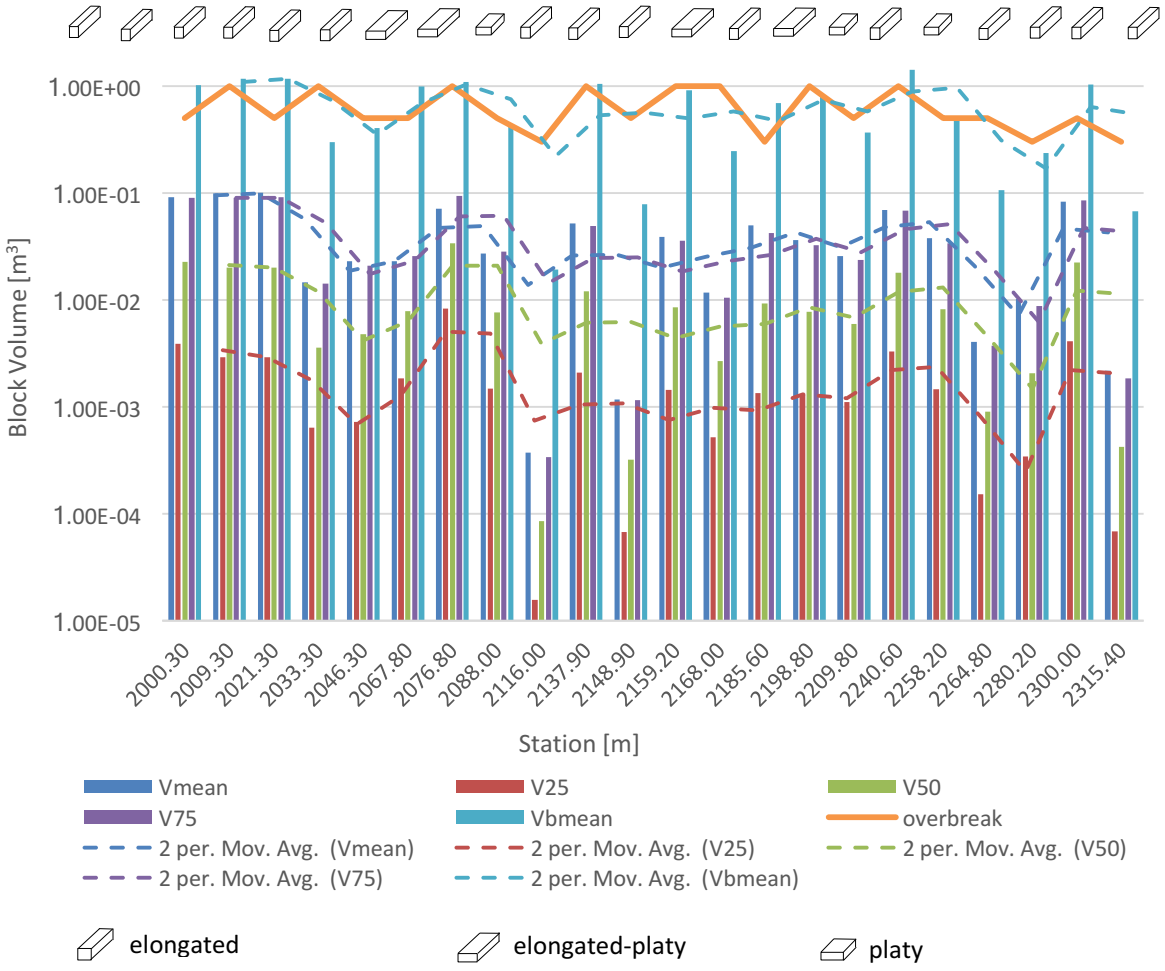

Figure 5.3: Theoretical IBSD and BSD compared with documented overbreak along the investigated tunnel sections.

By analysing Figure 5.3, similar curve progressions of determined block volumes and documented overbreak are apparent. This enhances the assumption, that with decreasing mean block volumes, overbreak also decreases and vice versa. A further potential indicator for overbreak was determined to be the dominating block shapes of individual sections. Which, however, cannot be seen in the correlation matrix. But this might be due to the fact, that the correlation matrix does not consider trends in the block shape classes.

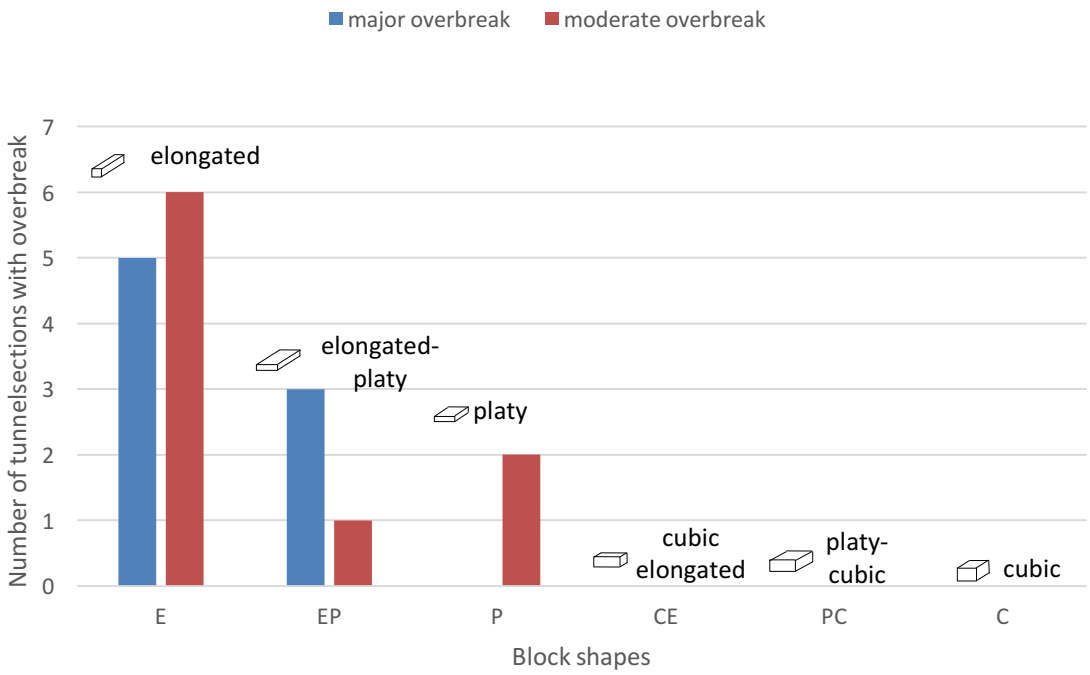

Figure 5.4: Block shapes compared to the occurrence of major and moderate overbreak for individual tunnel sections.

Figure 5.4 shows the relation of documented overbreak, to different block shapes. As no numerical correlation was determined with the correlation study, an intuitive comparison of documented overbreaks with their corresponding block shape was done. By analysing this, one can assume that there is an obvious tendency for overbreak to happen in rock masses dominated by very elongated blocks. However, as the entire investigated rock mass is dominated by long, elongated blocks, this assumption may not apply for different block size distributions as well. Furthermore, an investigation of 22 tunnel sections might not deliver representative results, as it might not be sufficient to make general statements about specific rock mass behaviours.

5.4 Correlation matrix

As mentioned in chapter 3.4.1, correlation values higher than |0.5| were assumed to indicate a correlation and are therefore analysed in this work. First of all, correlation values higher than |0.7| between the calculated volume and area to the design cross section, confirm the validity of the applied method, since the single parameters are dependent on each other, the same counts for the computed block sizes and the joint normal spacing. Second, a positive correlation of 0.52 between the DoF and UCS was identified. As it is known, that the degree of fracturing is directly related to primitive field stresses, one could assume that these different DoF of the investigated tunnel sections were caused by significant

differences of the overburden. However, as the overburden along the investigated tunnel sections nearly remained constant with differences of about 45 m, one could exclude the change of DoF due to initial stresses. Therefore, one can assume that in rock mass materials with higher compressive strengths tend to show a higher DoF. However, both values might also be determined in advance rather than onsite and be chosen according to the previous design stage (preliminary studies).

Furthermore, the correlation matrix showed no correlation of documented faults with other parameters at all. Hence, one could assume that faults do not influence underground excavation in terms of the investigated factors. However, this can be explained due to the small dimensions of the faults, which occurred in the investigated tunnel sections. These effects are restricted very local, and hence have just a small influence onto the excavation behaviour, which might be an explanation that they have not been identified.

Moreover, the matrix showed poor correlation of $V_{b,mean}$ with A, $V$and A_D, which indicates that there is no influence of the mean block size onto the calculated and documented tunnel dimensions. However, as depicted in Figure 4.10, a positive correlation between $V_{b,mean}$ and the documented overbreak could be determined. This indicates that increasing block volumes lead to larger overbreaks. Furthermore, a positive correlation between overbreak and the specific amount of explosives $E_{ob,-1}$ could be determined as well. Thus, the assumption can be made, that higher specific amounts of explosives lead to higher overbreaks. Consequently, $E_{ob,-1}$ correlates with A, $V$and A_D as well, as higher amounts of explosives lead to higher excavation volume. Moreover, the negative correlation of $E_{ob,-1}$with N_{tot}/A confirms that a higher number of joints lead to a lower required amount of explosives. Positive correlations of $E_{ob,+1}$ with $E_{ob,-1}$, A, $V$and A_D indicate a similar trend of the continuous adaption of the amount of explosives used for corresponding successive blasting rounds. Another positive correlation was determined between median values of joint normal spacings and the DOF. Hence, the remote, objective approaches for the identification of the joint spacing deliver similar results, as the subjective estimation of the DoF from a geologist. As no parameters showed correlation with the number of installed bolts, a pre-defined bolt pattern could be assumed. Nonetheless, only a 315 m long section, consisting of 22 tunnel faces was analysed and hence used for the correlation matrix. This is a rather small sampling volume and it would be interesting, if a larger amount of data respectively more cross-sections would confirm the found results or indicate other correlations, which were undetected at this stage.

6 Conclusion

This study presents the characterization of a joint network, including the IBSD and the BSD, in a tunnel section of 315 m in length. Aim was the investigation of the influence of the joint network geometry on the excavation with respect to overexcavation and explosives consumption. Possible factors controlling overbreak were identified by introducing a correlation matrix, where several different determined and documented parameters were put into relation with each other.

The characterization of the joint network was done by using three different discontinuity identification methods (both vector- and pixel-based). Basis for all three approaches were the digital surface models of the investigated tunnel sections. In all analysed sections, the identified sets that fitted best to the geological documentation were chosen for further investigations. This process delivered reproducible results in a very high quantity and accuracy regarding the set orientations and spacing. For the determination of the IBSD as well as the BSD, numerical models, using the obtained joint network characteristics, were created. In a subsequent step, it was possible, to determine the theoretical in situ block size and shape distributions. Additionally, a kinematic analysis of each tunnel section was performed, using the application VisKBT (Shi., 2017), in order to identify unstable blocks. The information about the joint network geometry, instable blocks and information from the geological documentation were fed into a correlation matrix, to search for correlating factors. Although the semi-automatically identified joint sets showed good accordance with the manually mapped ones, with median deviations of ± 12° for dip direction and ± 8° for dip angle, one must consider that three different identification methods were necessary to achieve these results.

The correlation matrix showed that there is a good correlation of documented overbreak with the consumption of explosives used for one blasting round, as well as the mean block volume. Hence, the assumption can be made, that higher amounts of explosives as well as higher mean block volumes may be causes for major overbreaks. Furthermore, a negative correlation of $E_{ob,-1}$with N_{tot}/A confirms the assumption, that more fractures lead to a reduced amount of explosives, as the blasting energy, used for one round length, decreases with an increasing degree of fracturing.

Other parameters, however, only show weak correlation, which might be due to a too small number of investigated cross-sections, or an incorrect identification of various parameters.

Bibliography

3GSM GmbH. (2018). ShapeMetriX3D. 3D imaging for measuring and assessing rock and terrain surfaces. Retrieved from www.3gsm.at.

Aichinger. (2018). *Determination of the Block Size and Shape Distribution in a Quarry by using Remote Sensing Techniques*. Graz University of Technology.

Austrian Society for Geomechanics. (2010). Guideline for the Geotechnical Design of Underground Structures with Conventional Excavation, 29.

Barton, N., Lien, R., & Lunde, J. (1974). Engineering classification of rock masses for the design of tunnel support. *Rock Mechanics Felsmechanik Mécanique Des Roches*. https://doi.org/10.1007/BF01239496

Bieniawski, Z. T. (1973). Engineering Classification of Jointed Rock Masses. *Civil Engineer in South Africa*. https://doi.org/http://dx.doi.org/10.1016/0148-9062(74)92075-0

Buyer, A., Pischinger, G., & Schubert, W. (2018). *Image-based Discontinuity Identification*.

Buyer, A., Sc, M., Graz, U., Pischinger, G., Gmbh, G. Z. T., Schubert, W., & Graz, T. U. (2017). Neue Möglichkeiten der Gebirgscharak- terisierung im Tunnelbau – Ein Beispiel vom Gleinalmtunnel.

Buyer, A., & Schubert, W. (2017). Calculation the Spacing of Discontinuities from 3D Point Clouds. *Procedia Engineering*, *191*, 270–278. https://doi.org/10.1016/j.proeng.2017.05.181

Buyer, A., & Schubert, W. (2018). Joint Trace Detection in Digital Images, (July).

Datamine, & CSIRO. (2018). Sirovision. Retrieved from http://www.dataminesoftware.com/sirovision/

Deere, D. U., & Deere, D. W. (1963). The Rock Quality Designation (RQD) Index in Practice. *Rock Classification Systems for Engineering Purposes*. https://doi.org/10.1520/STP48465S

Dr. Gen-hua Shi. (2017). VisKBT. Shenzhen: Engineering Computing Center, University of Chinese Academy of Sciences. Retrieved from http://www.ddamm.org/wiki/Softwares#VisKBT

EN ISO 14689-1. (2016). Geotechnische Erkundung und Untersuchung - Benennung, Beschreibung und Klassifizierung von Fels - Teil 1: Benennung und Beschreibung (ISO/DIS 14689-1:2016).

Fairhurst, C., & Damjanac, B. (1996). The excavation damaged zone – an international perspective. *Proceedings of the Excavation Disturbed Zone Workshop – Designing the Excavation Disturbed Zone for a Nuclear Waste Repository in Hard Rock, Canadian Nuclear Society, Manitoba, Canada (1996)*, 4–14.

Franklin, J. A., Maerz, N. H., & Brennet, C. P. (1988). Rock mass characterization using

photoanalysis. *International Journal of Mining and Geological Engineering*, *6*(2), 97–112.

Gaich, A., & Pischinger, G. (2016). 3D images for digital geological mapping. *Geomechanics and Tunnelling*, *9*(1), 45–51. https://doi.org/10.1002/geot.201500048

Gaich, A., Pötsch, M., & Schubert, W. (2017). Digital rock mass characterization 2017 – Where are we now? What comes next? *Geomechanik Und Tunnelbau*, *10*(5), 561–566. https://doi.org/10.1002/geot.201700036

Geoconsult ZT GmbH. (2015). *A9 Pyhrn Autobahn, Vollausbau Gleinalmtunnel, Geologische Tunneldokumentation abfalltechnische Beurteilung und wasserwirtschaftliche Beweissicherung, Geologische Tunneldokumentation: Schlussbericht, Salzburg.*

Girardeau-Montaut, D. (2018). CloudCompare. 3D point cloud and mesh processing software. Retrieved from https://www.danielgm.net/cc/

Goodman, R. E., & Shi, G. (1985). *Block Theory and its Application to Rock Engineering*. *Engineering Geology*. California. https://doi.org/10.1016/0013-7952(88)90010-5

Gottsbacher, L. (2017). Calculation of the Young ' s Modulus for Rock Masses with 3DEC and comparing it with empirical methods, (September).

Hoek, E., & Diederichs, M. S. (2013). Quantification of the Geological Strength Index Chart. *47th US Rock Mechanics / Geomechanics Symposium Held in San Francisco, CA, USA June 23-26, 2013*, 9.

Hoek, E., Kaiser, P. K., & Bawden, W. F. (1995). Support of Underground Excavations in Hard Rock, 240. Retrieved from https://books.google.ru/books?id=RefFNXdxt7wC

ISRM. (1978). Suggested Methods - Quantitative Description of Discontinuities.

Itasca Consulting Group. (2007). 3DEC - 3 Dimensional Distinct Element Code.

Itasca Consulting Group. (2018). 3DEC: 3 Dimensional Distinct Element Code. Modeling software. Minnesota: Group, Itasca Consulting. Retrieved from https://www.itascacg.com/software/3dec

Jouanna, P., Armangau, C., Batchelor, A. S., Bonazzi, D., Bruel, D., Ledoux, E., … Valla, P. (1993). *9 - A Summary of Field Test Methods in Fractured Rocks*. *Flow and Contaminant Transport in Fractured Rock*. https://doi.org/http://dx.doi.org/10.1016/B978-0-12-083980-3.50013-9

Kalenchuk, K. S., Diederichs, M. S., & McKinnon, S. (2006). Characterizing block geometry in jointed rockmasses. *International Journal of Rock Mechanics and Mining Sciences*, *43*(8), 1212–1225. https://doi.org/10.1016/j.ijrmms.2006.04.004

Kim, B. H., Cai, M., Kaiser, P. K., & Yang, H. S. (2007). Estimation of block sizes for rock masses with non-persistent joints. *Rock Mechanics and Rock Engineering*, *40*(2), 169–192. https://doi.org/10.1007/s00603-006-0093-8

Kluckner, A. (2015). Estimation of the in situ block size in jointed rock masses using three-dimensional block simulations and disconti ...., (July).

Palmstrom, A. (2005). Measurements of and correlations between block size and rock quality designation (RQD). *Tunnelling and Underground Space Technology*, *20*(4), 362–377. https://doi.org/10.1016/j.tust.2005.01.005

Palmström, A. (1982). The volumetric joint count—A useful and simple measure of the degree of jointing. In *IVth International Congress IAEG*.

Palmström, A. (1995). RMi - a system for characterizing rock mass strength for use in rock engineering. *Journal of Rock Mechanics and Tunnelling Technology*, *1*(2), 1–40. https://doi.org/10.1016/0886-7798(96)00015-6

Palmström, A. (2000). Block Size and Block Size Distribution. *GeoEng2000 Conference*, (November), 18–24.

Palmström, A. (2001). Measurement and characterizations of rock mass jointing. *In-Situ Characterization of Rocks - Chapter 2*, 1–40.

Palmström, A. (2002). Rock discontinuities 4.1.

Palmstrom, A., & D, P. (2005). Measurements of and Correlations between Block Size and Rock Quality Designation (RQD), *20*, 362–377.

Riquelme, A. (2016). DSE. Retrieved from https://sourceforge.net/projects/discontinuity-set-extractor/

Riquelme, A. J., Abellán, A., Tomás, R., & Jaboyedoff, M. (2014). A new approach for semi-automatic rock mass joints recognition from 3D point clouds. *Computers and Geosciences*, *68*, 38–52. https://doi.org/10.1016/j.cageo.2014.03.014

Riquelme, A., Tomás, R., Cano, M., Abellán, A., Tomás, R., & Abellán, A. (2016). Using open-source software for extracting geomechanical parameters of a rock mass from 3D point clouds: Discontinuity Set Extractor and SMRTool. *Rock Mechanics & Rock Engineering: From the Past to the Future*, *2*(October), 1091–1096. https://doi.org/doi:10.1201/9781315388502-190

Singhal, B. B. S., & Gupta, R. P. (2010). Applied hydrogeology of fractured rocks: Second edition. *Applied Hydrogeology of Fractured Rocks: Second Edition*, 1–408. https://doi.org/10.1007/978-90-481-8799-7

Söllner, P. (2014). *Determination of the in situ Block Size Distribution as a Parameter for the Rock Mass Characterization based on Measurements and Statistical Methods*. Graz University of Technology. Retrieved from www.tunnel.tugraz.at

Appendix A

This appendix displays the results of the correlation study including the input parameters (Figure 6.1) and the correlation matrix Figure 6.2).

Section	Av p. sp.	A SMX	A Mat.	V	AD	Drill. vis.	A/AD	V/AD	DoF	UCS	System	Fault	Vmean	V25	V50	V75	Vmin	Vmax	Abmean	Vbmean	BS	Ntcd/V	V/A	Ntcd/A	EOB-1	EOB-1	EOB-1	bund Lengt	NU.tot.	FJ.med	SJ.med	Key	Potential	Anchors	Overburd.
2000.30	0.02	155.10	125.83	134.67	85.00	0.70	1.48	1.58	2.00	2.00	0.50	0.00	9.13E-02	3.89E-03	2.25E-02	9.02E-02	7.98E-11	3.27E+00	1.66E+00	1.02E+00	1.00	5.61	1.07	6.01	3.02	770.50	2.62	667.90	3.00	756.00	1.52	0.38	8	3	5.00	304.10
2009.30	0.03	182.70	131.79	169.76	85.00	0.60	1.55	2.00	2.00	2.00	1.00	1.00	9.87E-02	2.89E-03	1.99E-02	8.38E-02	3.36E-11	3.60E+00	2.13E+00	1.16E+00	1.00	4.71	1.29	6.07	2.79	712.00	2.87	733.30	3.00	800.00	1.05	0.37	4	7	8.00	306.40
2021.30	0.03	162.20	132.54	155.52	85.00	0.70	1.56	1.83	2.00	2.00	0.50	0.00	9.95E-02	2.90E-03	2.00E-02	9.08E-02	4.44E-11	3.63E+00	2.14E+00	1.17E+00	1.00	0.73	1.17	0.86	2.61	666.80	2.82	720.10	3.00	114.00	1.05	0.19	9	2	5.00	308.90
2033.30	0.02	114.70	88.23	101.34	55.60	0.70	1.59	1.82	2.00	3.00	1.00	1.00	1.45E-02	6.34E-04	3.56E-03	1.41E-02	8.02E-12	5.70E-01	5.07E-01	2.99E-01	1.00	5.63	1.15	6.47	2.62	437.63	2.98	496.70	3.00	571.00	1.08	0.33	6	5	5.00	311.10
2046.30	0.03	105.90	86.28	95.03	55.60	0.80	1.55	1.71	3.00	3.00	0.50	0.00	2.29E-02	7.24E-04	4.78E-03	2.08E-02	3.69E-12	9.60E-01	7.31E-01	4.02E-01	1.00	6.47	1.10	7.13	2.84	395.10	2.38	330.20	2.50	615.00	1.68	0.24	4	7	5.00	312.70
2067.80	0.02	194.40	130.99	150.24	85.00	0.90	1.54	1.77	2.00	2.00	0.50	0.00	2.30E-02	1.83E-03	7.85E-03	2.56E-02	4.79E-07	4.73E-01	1.73E+00	9.84E-01	1.00	6.70	1.15	7.68	2.16	551.80	2.59	659.70	3.00	1006.00	0.98	0.64	9	2	5.00	313.70
2076.80	0.02	152.80	121.55	142.69	85.00	0.00	1.43	1.68	2.00	2.00	1.00	0.00	7.13E-02	8.23E-03	3.38E-02	9.40E-02	3.56E-11	1.04E+00	1.27E+00	1.08E+00	2.00	6.93	1.17	8.14	2.78	709.20	2.08	530.20	3.00	980.00	1.25	0.58	6	5	5.00	314.30
2088.00	0.02	59.58	85.45	97.62	55.60	0.80	1.54	1.76	3.00	3.00	0.50	0.50	2.72E-02	1.47E-03	7.64E-03	2.94E-02	3.22E-12	9.35E-01	6.62E-01	4.19E-01	2.00	7.97	1.14	9.11	2.71	331.40	3.20	391.10	2.20	778.00	1.37	0.61	7	4	8.00	315.10
2116.00	0.02	62.43	91.51	103.04	55.60	0.80	1.65	1.85	3.00	3.00	0.30	0.50	3.73E-04	1.55E-05	8.46E-05	3.40E-04	5.03E-14	2.12E-02	3.31E-02	1.90E-02	3.00	8.96	1.13	10.09	2.30	281.10	3.21	267.50	2.20	923.00	3.09	0.09	6	5	0.00	318.80
2137.90	0.03	88.98	113.28	130.19	83.10	0.90	1.36	1.57	3.00	2.00	1.00	0.50	5.16E-02	2.07E-03	1.21E-02	4.89E-02	9.31E-11	1.94E+00	1.79E+00	1.05E+00	1.00	4.62	1.15	5.31	3.40	622.20	2.82	516.00	2.20	601.00	2.34	0.27	4	7	10.00	322.80
2148.90	0.03	96.11	134.13	148.81	83.10	0.90	1.61	1.79	3.00	2.00	0.50	0.50	1.16E-03	6.75E-05	3.19E-04	1.15E-03	1.20E-11	4.67E-02	1.28E-01	7.79E-02	1.00	1.03	1.11	1.14	2.91	532.00	2.30	420.20	2.20	153.00	1.13	0.37	10	1	9.00	325.00
2159.20	0.02	69.28	98.19	108.27	55.60	0.80	1.77	1.95	3.00	2.00	1.00	0.00	3.86E-02	1.44E-03	8.50E-03	3.56E-02	2.42E-10	1.37E+00	1.63E+00	9.12E-01	1.00	3.00	1.10	3.31	3.87	473.10	3.25	398.00	2.20	325.00	1.30	0.24	10	1	7.00	327.00
2168.00	0.02	71.01	99.69	102.54	55.60	0.80	1.79	1.84	2.00	2.00	1.00	1.00	1.17E-02	5.21E-04	2.68E-03	1.05E-02	1.48E-11	7.56E+01	4.28E-01	2.44E-01	2.00	7.15	1.03	7.35	2.64	322.90	3.31	405.30	2.20	733.00	0.31	0.30	4	7	7.00	328.80
2185.60	0.02	61.25	88.99	102.37	55.60	0.70	1.60	1.84	2.00	2.00	0.30	0.50	4.95E-02	1.33E-03	9.20E-03	4.23E-02	2.32E-12	2.66E+00	1.35E+00	6.91E-01	1.00	6.55	1.15	7.54	2.50	305.70	1.46	178.60	2.20	671.00	0.98	0.29	10	1	7.00	332.40
2198.80	0.03	59.70	87.42	105.66	55.60	0.50	1.57	1.90	2.00	2.00	1.00	0.50	3.62E-02	1.29E-03	7.89E-03	3.22E-02	5.17E-12	1.80E+00	1.43E+00	7.94E-01	2.00	6.49	1.21	7.85	2.18	266.90	2.75	336.30	2.20	686.00	1.64	0.20	6	5	7.00	334.80
2209.80	0.02	61.01	87.75	100.93	55.60	0.70	1.58	1.82	2.00	2.00	0.50	0.00	2.57E-02	1.10E-03	5.92E-03	2.36E-02	3.48E-12	1.48E+00	6.30E-01	3.66E-01	3.00	8.73	1.15	10.04	2.70	329.60	2.31	282.70	2.20	881.00	1.19	0.43	7	4	6.00	336.60
2240.60	0.02	74.72	100.23	110.49	55.60	0.80	1.80	1.99	2.00	2.00	1.00	1.00	6.90E-02	3.28E-03	1.78E-02	6.80E-02	4.07E-11	2.44E+00	2.35E+00	1.41E+00	1.00	5.21	1.10	5.75	3.51	429.00	2.20	268.80	2.20	576.00	1.23	0.55	10	1	6.00	338.90
2258.20	0.02	139.60	97.30	110.06	55.60	0.70	1.75	1.98	2.00	2.00	0.50	1.00	3.76E-02	1.46E-03	8.17E-03	3.36E-02	5.99E-12	2.14E+00	9.63E-01	5.12E-01	3.00	8.86	1.13	10.02	2.49	304.60	1.81	221.20	2.20	975.00	0.64	0.41	7	4	6.00	338.90
2264.80	0.02	71.10	91.79	105.37	55.60	0.80	1.65	1.90	3.00	2.00	0.50	1.00	4.05E-03	1.51E-04	8.95E-04	3.70E-03	3.24E-13	2.03E-01	1.88E-01	1.06E-01	1.00	8.90	1.15	10.22	1.90	232.10	1.51	184.70	2.20	938.00	1.50	0.19	5	6	7.00	346.60
2280.20	0.02	64.84	96.53	115.89	55.60	0.60	1.74	2.08	3.00	3.00	0.30	0.50	1.01E-02	3.42E-04	2.05E-03	8.95E-03	8.79E-12	4.69E-01	4.48E-01	2.35E-01	1.00	6.94	1.20	8.33	2.00	244.70	2.14	261.10	2.20	804.00	1.51	0.21	4	7	6.00	351.50
2300.00	0.02	67.41	95.96	109.50	55.60	0.50	1.73	1.97	3.00	3.00	0.50	0.50	8.26E-02	4.07E-03	2.22E-02	8.47E-02	3.37E-11	2.91E+00	1.71E+00	1.03E+00	1.00	8.63	1.14	9.85	2.37	289.40	3.15	385.50	2.20	945.00	1.12	0.55	6	5	7.00	357.10
2315.40	0.03	65.46	96.26	123.20	55.60	0.40	1.73	2.22	3.00	3.00	0.30	0.00	2.17E-03	6.83E-05	4.22E-04	1.85E-03	2.41E-13	1.30E-01	1.30E-01	6.76E-02	1.00	2.54	1.28	3.25	2.46	770.50	2.21	667.90	1.93	313.00	1.55	0.19	8	3	5.00	352.57

Figure 6.1 Determined and form the geological documentation derived Parameters for the correlation study.

Figure 6.2: Correlation matrix with values higher than |0.5| highlighted in green, and higher than |0.4| highlighted in orange.